Chapter 2

Pulsed field gradients in high resolution NMR

2.1 Pulsed field gradients in NMR

The term *pulsed field gradient* is used for inhomogeneities of the static magnetic field caused by the switching of dc-currents in coils surrounding the sample region in a NMR spectrometer. The additional coils are usually designed such that the magnetic field B_0 they produce varies linearly over the sample region.

The use of pulsed field gradients had been suggested in 1963 in the context of diffusion measurements (McCall, 1963). The influence of self-diffusion on the spin-echo amplitude in the presence of a constant field gradient had already been discussed by Hahn in his original paper on spin echoes (Hahn, 1950). The gradients were caused by inhomogeneities of the static external field over the sample volume and the effect of diffusion on the spin echo amplitude was disturbing the intended measurement of spin-spin relaxation times. Separating relaxation from diffusion effects had been achieved by a modified pulse sequence suggested by Carr and Purcell (Carr and Purcell, 1954). This lead to a number of self-diffusion studies in viscous liquids (e.g. (McCall, 1963)), but it was realized that the measurement of smaller and smaller diffusion coefficients by constant field gradients became more and more unpractical. The use of pulsed field gradients and stimulated echos led to a huge increase of the sensitivity (Stejskal and Tanner, 1965). Frequency resolved spin-echo measurements had been suggested by Vold et al. (Vold, 1968) soon after the introduction of the Fourier transformation technique (Ernst and Anderson, 1966). An application to measure self-diffusion coefficients of different components in complex systems using pulsed field gradient Fourier transformation NMR followed (James and McDonald, 1973). This combination lead to wide spread applications in different parts of NMR (Callaghan, 1991).

During a constant field gradient, the static magnetic field varies across the sample. The Larmor frequency of a single resonance line is directly proportional to the position within the sample. This effect can be used to obtain an image of the spin density. This idea due to Lauterbur (Lauterbur, 1973) was the starting point of spatially resolved magnetic resonance techniques with applications in biology, medicine and material sciences (Blümich, 1998; Callaghan, 1991; Kimmich, 1997; Miller, 1998; Vlaardingerbroek and denBoer, 1996).

The potential use of pulsed field gradients to perform signal selection in high-resolution spectroscopy has been recognized in 1978 (Maudsley, 1978). Their routine use in multi-dimensional NMR experiments was pioneered by Hurd (Hurd, 1990). This development was triggered by the invention of actively shielded gradient coils. A rigorous theoretical treatment of signal selection by pulsed field gradients was given by Mitschang et al. (Mitschang, 1994; Mitschang, 1999). The finding of an optimal sequence of pulsed field gradients for any NMR experiment has been reduced to a geometrical problem. The development and application of a computer program based on this theory is part of the underlying thesis. The results are discussed in (Thomas, 1999) as well as in paragraph 2.3.

Paragraph 2.2 gives an outline of the theory, which includes the discussion of coherent motion and diffusion on the signal amplitude in a multi-pulse heteronuclear experiment with pulsed field gradients. The geometric formulation of pathway selection of Mitschang et al. is reproduced. The design of gradient pulse sequences is discussed in detail in prepublished work (Thomas, 1999). Paragraph 2.3 gives additional information on the treatment of pulse imperfections and optimizing water suppression. Paragraph 2.4 discusses signal loss by diffusion.

2.2 Theory

High-resolution multi-pulse heteronuclear experiments on liquid samples are most conveniently discussed in terms of the product operator formalism (Ernst, 1987; Sorensen, 1983). In the course of a NMR experiment, coherence is transferred between nuclei, and superpositions of eigenstates of the spin system are excited. These superpositions are conveniently classified into coherence orders p, standing for the difference in the magnetic quantum numbers of the contributing eigenstates [for a comprehensive discussion see for example (Levitt, 1988)]. The concept of coherence order is particularly important in the description of experiments with pulsed field gradients during free evolution intervals.

The Hamiltonian, which describes the interaction of a heteronuclear spin system with a pulsed field gradient, is

$$\mathsf{H}_G(t) = -g(t)\left[\sum_i r_i(t)\gamma_I I_z^i + \sum_i r_i(t)\gamma_S S_z^i)\right] \qquad \textbf{(2.1)}$$

where **g** = gradB(t) is the time dependent pulsed field gradient, $\mathbf{r}_i$ the position of the nuclear spin i, and I_z and S_z the Cartesian spin operators of species I (protons) and S (heteronucleus) with the gyromagnetic ratios γ_I and γ_S. (For simplicity, only one heteronuclear species is considered explicitly. If it becomes necessary, a generalization of the equation to treat more than two different spin species can easily be done.) The sum extends over all nuclear spins in the sample.

The Hamiltonian in this form contains the position of all spins as a function of time. However, we are dealing with a liquid in a steady state of thermal motion. The motion of the nuclear spins is a random process, and we have to introduce probability concepts to describe the position of the spins. Brownian motion is a stochastic process evolving in continuous time, and so we define a family of random variables R_t, parameterized by the time t, and let r_t denote the values taken by R_t (Gardiner, 1983).

The smallest length scale which can be sensed by pulsed field gradients is typically of the order of μm (Callaghan, 1991). The size of the molecules in liquid NMR experiments does not exceed a few nm. Therefore, the stochastic variables R_t^i are taken to describe the motion of the center of mass of molecule i. Internal motions or overall rotation of the molecule are neglected. In cases where the molecule gets extremely big or the gradients very strong, additional internal variables have to be included in the description.

The Hamiltonian then is

$$\mathsf{H}_G(t) = -g(t)\left[\sum_i R_t^i(\sum_j \gamma_I I_z^j + \gamma_S S_z^j)\right] \qquad \textbf{(2.2)}$$

with the first sum extending over all molecules in the sample, and the second sum including each spin of one molecule.

This Hamiltonian induces a spatially dependent precession of the spins in the transverse plane. The precession frequency depends on the coherence order p and the phase shift induced by a pulsed field gradient during a time interval r is given by

$$(\gamma_I p_I^r + \gamma_S p_S^r)\mathbf{g}(t)\mathbf{R}_t^i \qquad \textbf{(2.3)}$$

with the coherence orders p_I^r and p_S^r of the spins I and S present during the time interval r. The different coherence orders excited during the experiment can be collected in a coherence transfer pathway with an overall phase shift

$$\varphi_i(t) = \int_0^t \mathbf{g}^*(t')\ \mathbf{R}_t^i\ dt' \qquad \textbf{(2.4)}$$

with the effective gradient g^* being introduced to take care of the different coherence orders during the experiment for simplicity purpose. The explicit form of the dependence of the effective gradient on the coherence orders and gradient strengths will be specified later. The detected signal of the NMR experiment is proportional to the ensemble average

$$S(\mathbf{g}^*) = \sum_i \left\langle e^{i\varphi_i(t)} \right\rangle_L = \sum_i \int_0^t dt \int_{\mathbf{r}_t^i \in V} d\mathbf{r}_t^i\ P(\mathbf{r}_t^i, t \mid \mathbf{r}_0^i, 0) p(\mathbf{r}_0^i, 0) \exp\{i\ \mathbf{g}^*(t)\ \mathbf{r}_t^i\} \qquad \textbf{(2.5)}$$

with the conditional probability density

$$P(\mathbf{r}_t^i, t \mid \mathbf{r}_0^i, 0) d\mathbf{r}_t^i \equiv \mathrm{Prob}(\mathbf{r}_t^i \le \mathbf{R}_t^i < \mathbf{r}_t^i + d\mathbf{r}_t^i \mid \mathbf{R}_0^i = \mathbf{r}_0^i) \qquad \textbf{(2.6)}$$

In the notation of (2.5), the stochastic process is defined by a family of random variables $\mathbf{R}_t^i$ in continuous time. No further assumptions are made at this point about the nature of the process. The ensemble average over the time integral of the phase accumulated by a molecule i is defined by taking the ensemble average for each t, where the Integral $\mathbf{r}_t^i$ extends over all possible values that $\mathbf{r}_t^i$ can take. This ensemble-averaged quantity is then time integrated and the overall signal of the NMR experiment is obtained by a summation of the contribution of each molecule.

The spatial average in (2.5) can be analyzed using the cumulant expansion theorem (Stepisnik, 1981):

$$\left\langle \mathbf{e}^{i\varphi_i(t)} \right\rangle_L = \mathbf{e}^{\left(i\langle\varphi_i(t)\rangle_L - \beta_i(t) + \ldots\right)} \qquad \textbf{(2.7)}$$

This corresponds to an expansion about the mean value

$$\left\langle \varphi_i(t) \right\rangle_L = \int_0^t \mathbf{g}^*(t')\ \left\langle \mathbf{R}_t^i \right\rangle_L\ dt' \qquad \textbf{(2.8)}$$

The attenuation exponent β_i is given by

$$\beta_i(t) = \frac{1}{2}\int_0^t\int_0^t \mathbf{g}^*(t')\left\langle \mathbf{R}_{t'}{}^i\mathbf{R}_{t''}{}^i\right\rangle_{LC}\mathbf{g}^*(t'')dt'dt'' \qquad \textbf{(2.9)}$$

In Eq. (2.9) the local correlation (Callaghan, 1991) or second order cumulant

$$\left\langle \mathbf{R}_{t'}{}^i\mathbf{R}_{t''}{}^i\right\rangle_{LC} = \left\langle \mathbf{R}_{t'}{}^i\mathbf{R}_{t''}{}^i\right\rangle_{L} - \left\langle \mathbf{R}_{t'}{}^i\right\rangle_{L}\left\langle \mathbf{R}_{t''}{}^i\right\rangle_{L} \qquad \textbf{(2.10)}$$

is introduced.

For a Gaussian phase distribution all cumulants of higher order than 2 vanish (Gardiner, 1983). The local correlation is in that case equal to the variance σ of the probability density. For a typical high resolution NMR setup the molecules inside the sample diffuse freely, which means that the molecules do not hit any barrier during the experiment. In this case the phases in (2.8) are Gaussian distributed and no higher order corrections need to be applied. In cases of restricted diffusion in microstructures, the Gaussian assumption or, as it is often termed in view of a Stejskal-Tanner type diffusion experiment, the narrow-pulse criterion has to be checked carefully (Wang, 1995).

The oscillatory part of the signal in (2.5) arises from the mean spin displacement. The motion of the mean spin displacement can be expanded in powers of time (Callaghan, 1991)

$$\left\langle \varphi_i(t)\right\rangle_L = \mathbf{r}\int_0^t \mathbf{g}^*(t')\ dt' + \mathbf{v}\int_0^t t'\mathbf{g}^*(t')\ dt' + \frac{1}{2}\mathbf{a}\int_0^t t'^2\mathbf{g}^*(t')\ dt' + ... \qquad \textbf{(2.11)}$$

Where **r** is the average spin position in the sample measured from the origin of the gradient coordinate system, **v** and **a** are the mean velocity and the mean acceleration. This expansion presupposes that all spins in the sample have a common average motion. In the case of a stagnant fluid only the first term of the expansion remains. If the time integral over the effective gradient - hereafter referred to as the average gradient - is vanishing, the signal phase does not depend on the position **r** of a molecule. Therefore all molecules within the sample contribute with equal phase to the signal. The signal is named "gradient echo" if the effective gradient is different from zero during part of the time.

In cases where the average gradient is nonzero, the signal phase will encode for the position of the spins within the sample. Recording a series of consecutive experiments in which the average gradient is increased linearly from zero to a large value (or in practice from a large negative to a large positive value) leads to a diffraction type of signal modulation. The Fourier transform of the signal is a direct representation of the projection of the spin density within the sample on the gradient direction. This linear sampling of the signal decay in dependence of the average gradient is used extensively in NMR imaging.

In high resolution NMR spectroscopy, the goal is to form a gradient echo for the signal of interest. To evaluate the refocusing condition, the effective gradient has to be specified explicitly. In a multi-pulse high resolution NMR experiment, the time integral of Eq. (2.11) is decomposed into different intervals of free precession separated by rf-pulses. During such an interval r, the coherence order is constant and Eq. (2.4)specifies the rate and sign of the gradient induced phase shift. The rf pulses induce changes of coherence order. With the exception of 180° pulses, each pulse changes the coherence order before the pulse into several new coherence orders after it. These new coherence orders, which accumulated the same gradient induced phase shift during the interval r, will collect different phase factors during the interval r+1 and have to be treated as separate terms. In this way, the rf-pulses create a multitude of coherence order transfer pathways. Each of these pathways will be influenced in a different manner by a sequence of pulsed field gradients. To evaluate Eq. (2.11), the average gradient for <u>one single</u> coherence pathway can be written as

$$\int_0^t \mathbf{g}^*(t')\,dt' = \begin{pmatrix} \sum_{r=1}^{F}\left(\gamma_I p_I^r + \gamma_S p_S^r\right) G_x^r \int_{\tau_r}^{\tau_r+\delta_r} f_x^r(t')\,dt' \\ \sum_{r=1}^{F}\left(\gamma_I p_I^r + \gamma_S p_S^r\right) G_y^r \int_{\tau_r}^{\tau_r+\delta_r} f_y^r(t')\,dt' \\ \sum_{r=1}^{F}\left(\gamma_I p_I^r + \gamma_S p_S^r\right) G_z^r \int_{\tau_r}^{\tau_r+\delta_r} f_z^r(t')\,dt' \end{pmatrix} \qquad \textbf{(2.12)}$$

The time integral is expressed as sum over all free evolution periods of the experiment. Pulsed field gradients are applied at times $\boldsymbol{\tau}_r$ with amplitudes $\mathbf{G}_\alpha^r$ (α=x,y,z) and shape factors $\mathbf{f}_\alpha^r$ in the interval **r** of the experiment during which the coherence orders $\mathbf{p}_I^r$ and $\mathbf{p}_S^r$ are excited. The shape factor f_α^r is a smooth function

with a maximum value of 1, which is non-zero only during the time interval $[\tau_r, \tau_r+\delta_r]$. F is the total number of free evolution intervals of the experiment. By further introducing the composite coherence order p (John, 1991; Mitschang, 1994) and the gradient strength s_α^r

$$p^r = p_I^r + \left(\frac{\gamma_I}{\gamma_S}\right) p_S^r \qquad \textbf{(2.13)}$$

$$s_\alpha^r = G_\alpha^r \int_{\tau_r}^{\tau_r+\delta_r} f_\alpha^r(t')\,dt' \qquad \textbf{(2.14)}$$

the condition for a vanishing average gradient reads

$$\int_0^t \mathbf{g}^*(t')\;dt' = \gamma_I \begin{pmatrix} \sum_{r=1}^{F} p^r s_x^r \\ \sum_{r=1}^{F} p^r s_y^r \\ \sum_{r=1}^{F} p^r s_z^r \end{pmatrix} = \gamma_I \begin{pmatrix} \mathbf{ps_x} \\ \mathbf{ps_y} \\ \mathbf{ps_z} \end{pmatrix} = -\mathbf{k} = 0 \qquad \textbf{(2.15)}$$

with the gradient strengths along the Cartesian axes $\mathbf{s}_\alpha$ (α=x,y,z) and the composite coherence orders **p** written as a vector with F components. Eq. (2.15) defines the general wave vector **k**.

The resulting signal amplitude from the oscillating part in (2.5)

$$\frac{S(\mathbf{kr})}{S_0} = \frac{2J_1(k_r R)}{k_r R}\,\frac{\sin(k_z L)}{k_z L} \qquad \textbf{(2.16)}$$

where the sample volume is taken to be a cylinder of height L and radius R with uniform spin density. Its center is the origin of the coordinate system and its axis of cylindrical symmetry along the Zeeman field. The radial component of the wavevector is $k_r = (k_x^2 + k_y^2)^{1/2}$ (Mitschang, 1999; Thomas, 1999).

Eqs. (2.16) and (2.15) reduces the finding of an optimal gradient sequence for a given pulse sequence to a geometrical problem (Mitschang, 1994). The condition (2.15) has to be fulfilled for all selected coherence transfer pathways simultaneously, while the factor (2.16) should be as small as possible for all pathways to be suppressed. The solution of this multidimensional minimization problem is found with the aid of the

computer programs Z GRADIENT and TRIPLE GRADIENT and is discussed in more detail in section 2.3.2.

The second term in the expansion of Eq. (2.7) leads to a damping of the signal for all coherence pathways. This damping is caused by the statistical fluctuations of the average molecular motion. The location correlation in its general form of Eq. (2.10) is a second rank tensor.

The diffusion coefficient of a particle undergoing Brownian motion can be defined in two different ways. (1) In the phenomenological approach, a concentration gradient causes a particle current density **j** proportional to the concentration gradient **grad** c. The constant of proportionality is called the *diffusion constant* D (Fick's law). (2) The second approach is a microscopic approach. Here the self-diffusion tensor is defined as the spectral density function of the particle velocity auto-correlation:

$$D_{\alpha,\beta}(\omega) = \frac{1}{2}\int_{-\infty}^{\infty} \left\langle V_t^{\,i}{}_{\alpha} V_t^{\,i}{}_{\beta} \right\rangle_L e^{i\omega t} dt \qquad \textbf{(2.17)}$$

In the limit of zero frequency, the two definitions are equivalent for non-interacting Brownian particles (Ohtsuki and Okano, 1982). The relationship between the particle velocity auto-correlation and the local correlation is described in detail in (Callaghan, 1991). The result is

$$\left\langle \alpha_{t'}^{\,i} \alpha_{t''}^{\,i} \right\rangle_{LC} = \frac{1}{\pi}\int_{-\infty}^{\infty} D_{\alpha\alpha}(\omega)\, \frac{e^{i\omega(t'-t'')}}{\omega^2}\, d\omega \qquad \alpha = \text{x, y, z} \qquad \textbf{(2.18)}$$

In this case (2.9) might be expressed as (Stepisnik, 1981; Stepisnik, 1985)

$$\beta_i(t) = \sum_{\alpha=x,y,z} \frac{1}{2\pi}\int_{-\infty}^{\infty} \frac{D_{\alpha\alpha}(\omega)}{\omega^2} \left|\tilde{g}_{\alpha}^{*}(\omega, t)\right|^2 d\omega \qquad \textbf{(2.19)}$$

where the Fourier transform of the effective gradient

$$\tilde{g}_{\alpha}^{*}(\omega, t) = \int_0^t g_{\alpha}^{*}\, e^{i\omega t'} dt' \qquad \textbf{(2.20)}$$

has been introduced.

The attenuation factor in Eq. (2.19) depends on the spectral density of the translational motion and the squared spectrum of the effective gradient. The analogy between this expression and equations for spin relaxation has been pointed out by Callaghan (Callaghan, 1991; Callaghan and Stepisnik, 1995). In relaxation, the spectral density of the random rotational motion of the molecule is sampled at frequencies corresponding to the Larmor frequencies of the involved spins, their sum and difference. In a diffusion experiment the spectral density of the random translational motion is sampled with the function

$$S_\alpha(\omega, t) = \frac{\left|\tilde{g}_\alpha^*(\omega, t)\right|^2}{\omega^2} \qquad \textbf{(2.21)}$$

which is characteristic of the gradient spectrum. However, in terms of this analogy, we maneuver in the regime of extreme motional narrowing for aqueous protein solutions, e.g. the function $D_{\alpha\alpha}(\omega)$ can be replaced by $D_{\alpha\alpha}(0)$, which represents the self-diffusion coefficient along the Cartesian axis α. If a model of Brownian motion is assumed, the characteristic time scale for the motion will be the jump time of the random walk (Callaghan, 1991)

$$\tau_C \approx \frac{\sqrt{\left\langle V_t^{i\,2}{}_\alpha \right\rangle}}{D_{\alpha\alpha}(0)} \qquad \textbf{(2.22)}$$

which is of the order of pico-seconds for simple liquids. In contrast the fastest time scale of the gradient variation is typically not faster than a few μs, which is several orders of magnitude larger. Thus it is impossible to study spectral features of the translational motion in simple liquids or protein solutions.

The Parceval relation

$$\frac{1}{2\pi}\int_{-\infty}^{\infty} \frac{\left|\tilde{g}_\alpha^*(\omega, t)\right|^2}{\omega^2}\, d\omega \equiv \int_0^t \left|\int_0^u g_\alpha^*(t')\, dt'\right|^2 du \qquad \textbf{(2.23)}$$

in combination with Eqs. (2.5), (2.7) and (2.19), with D(ω) being replaced by D(0), gives two different general expressions of the signal attenuation due to diffusion. In the frequency domain, we get

$$\frac{S(\mathbf{s},\mathbf{p})}{S(\mathbf{s}=0)} = \exp\left\{ - \sum_{\alpha=x,y,z} \frac{1}{2\pi} D_{\alpha\alpha} \int_{-\infty}^{\infty} \frac{\left|\tilde{g}_\alpha^*(\omega,t)\right|^2}{\omega^2} \, d\omega \right\} \qquad \textbf{(2.24)}$$

and in the time domain, we get

$$\frac{S(\mathbf{s},\mathbf{p})}{S(\mathbf{s}=0)} = \exp\left\{ - \sum_{\alpha=x,y,z} D_{\alpha\alpha} \int_0^t \left| \int_0^u g_\alpha^*(t') \, dt' \right|^2 du \right\} \qquad \textbf{(2.25)}$$

Eqs. (2.24) and (2.25) describe the attenuation factor of one single coherence transfer pathway with the coherence orders represented by the vector **p** (see (2.13)) in an experiment with pulsed field gradients, the strength of which is represented by the vector **s** (see (2.14)). On the right hand side the explicit dependency on **p** and **s** is hidden in the effective gradient g^*. A general solution of this equation with an explicit representation of the effective gradient in terms of **p** and **s** and its implication to protein experiments will be discussed in paragraph 2.4. In case of a non-vanishing average gradient (2.12), the diffusion factor (2.24) or (2.25) has to be multiplied with the position dependent factor (2.16) to get the total attenuation due to the pulsed field gradients.

The result given in Eq. (2.25) reproduces earlier results (Kenkre, 1997; Stejskal and Tanner, 1965) which had been obtained by solving the classical Bloch-Torrey equations (Torrey, 1956).

2.3 Pathway selection and artifact suppression

2.3.1 General remarks

The selection of coherence transfer pathways is essential to any multi-pulse sequence. Depending on the coherence selection, the spectra obtained of an otherwise identical sequence of pulses can differ immensely. Selection of coherence transfer pathways can be done by phase cycling (Bain, 1984; Bodenhausen, 1984; Kessler, 1988). The pulse sequence, especially with the same time increment in a multidimensional experiment, is repeated a certain number of times only changing the phases of one or more of the pulses and the receiver. The signals of all scans are then added up in the receiver, where the wanted pathways accumulate, whereas the unwanted ones are cancelled by subtraction. This selection principle causes some problems:

1. Small changes in amplitude or phase between the scan lead to incomplete subtraction, causing so called t1-noise. Traces of noise appear as lines along the indirect dimensions at the detection frequency of large suppressed signals.
2. The FID acquired in a single scan contains all possible pathways of the experiment, which have to be fully digitized in the receiver. The choice of the receiver gain is often determined by large unwanted signals and small wanted signals are not digitized properly (*dynamic range*).
3. The measurement time can get exceedingly long, depending on the required number of scans to complete a phase cycle. This is especially inconvenient for concentrated samples, where one scan per time increment could often give a satisfying signal to noise ratio.

An alternative to the phase cycling is the pathway selection by pulsed field gradients. Whereas the selection via phase cycling is based on the change of coherence order, the effect of a pulsed field gradient is sensitive to the coherence order itself (2.3). The condition for refocusing a pathway is given in Eq. (2.15). It can be analyzed in a straightforward manner to get a gradient sequence that does not suppress any of the wanted pathways. However, it should be noted, that the refocusing of one or more wanted pathways is not sufficient for a selection. In order to perform a real selection, it must be made sure that all possible unwanted pathways are dephased at the same time by the gradient sequence. The finding of such a sequence is by no means trivial.

The main advantage of the use of pulsed field gradients is the fact that the selection procedure is done in one scan, which circumvents the problems of phase cycling mentioned above. On the other hand, there are major disadvantages of using pulsed field gradients as well:

1. The application of a pulsed field gradient induces eddy currents in any conductor near the coil.
2. A mechanical torque is applied to the gradient coil and thus to the probe. Both effects 1 and 2 disturb the stability of measurements.
3. The application of pulsed field gradients takes some extra time in many cases. This leads to loss of magnetization due to relaxation. Loss of magnetization due to diffusion is unavoidable as well.
4. If the wanted pathways are dephased before an amplitude type of magnetization transfer occurs during the experiment, half of the wanted pathways are lost and the signal intensity is reduced by a factor of 2 or $2^{½}$ (Mitschang, 1999).

Although the potential of the use of pulsed field gradients had been recognized very early on (Maudsley, 1978), the first point listed above has prevented the application in spectroscopy for a long time. The induced eddy currents can last long enough to inhibit the recording of a high-resolution spectrum for several hundred milliseconds

after the application of a pulsed field gradient. Thanks to the invention of actively shielded gradient coils (Mansfield and Chapman, 1986; Mansfield and Chapman, 1987; Turner and Bowley, 1986), the routine use of pulsed field gradients in spectroscopy was made possible. In their design, an additional shield coil is wound around the main gradient coil to compensate the field outside the sample volume. For such a coil design, eddy currents decay in times of the order of a hundred microseconds.

The problem of the mechanical disturbance is not so severe since the gradient strengths required for signal suppression are not very high. A typical problem induced by this force are vibrations of the sample, which might cause traces of t1 noise at a frequency of a few ten to hundred Hertz next to strong signals. Fixing the gradient coil tightly to the probe solves the problem.

The signal decay due to diffusion - which will be discussed in more detail in section 2.4 - is more of a problem for small molecules, which have long transverse relaxation times. For this class of molecules, some extra delay of one to three milliseconds does not affect the signal intensity very much. For large molecules though, the relaxation losses during such an interval might be intolerable. On the other hand the signal loss by diffusion can be neglected for large molecules.

The relaxation problem exists only for pulse sequences, which require a gradient during a delay that encodes the chemical shift in an indirect dimension. In those cases, the extra chemical shift evolution during the pulsed field gradient has to be refocused by a 180° Pulse. An alternative is to calculate the first points of the FID by linear prediction (Ross, 1993). This induces some artifacts of the lineshapes, if too many points have to be predicted.

The most severe problem in biological applications, where the signal to noise ratio of an experiment is crucial, is the signal reduction mentioned in point 4 above. Most multidimensional heteronuclear NMR experiments involve the transfer of magnetization via J-coupling evolution. Magnetization evolves from transverse in-phase magnetization I_x or I_y into antiphase magnetization I_yS_z or I_xS_z. The magnetization transfer is accomplished by a simultaneous 90° pulse on the I and S spins, which gives a rotation for the full antiphase magnetization that did build up

during the previous delay. Now the rest of the pulse sequence is designed to "work" only on the magnetization that has been rotated. Placing a pulsed field gradient into that interval will spread e.g. the I_yS_z part into equally distributed I_yS_z and I_xS_z, so that the following I_x pulse only rotates half of the initial antiphase magnetization, and since the pulse sequence is designed to continue working only on I_zS_y, the other half of the magnetization is lost (Muhandiram, 1994). The problem is circumvented, if the pulse sequence does continue working on both parts of the resulting magnetization as for example in a homonuclear isotropic TOCSY transfer. Thus gradients might be applied in these sequences without losing sensitivity (Sattler, 1995; Wijmenga, 1997).

The situation is different if a gradient is placed into an indirect evolution period. The magnetization precesses in the x-y plane while the indirect time domain is incremented and a subsequent 90° pulse flips only half of the magnetization on average. The resulting signal is amplitude modulated, which implies that the sign of the rotation during t1 is lost. To ensure that no scrambling occurs, the reference frequency has in principle to be placed to one side of the spectral region (Aue, 1976). However, methods have been developed, that circumvent this problem by shifting the phase of the pulses before the acquisition period (Marion, 1983; States, 1982). In this method the reference frequency can be placed in the center of the spectrum and an improvement by a factor $2^{½}$ in signal to noise ratio is reached by avoiding the folding of noise into the spectral region by the reduced spectral window. If gradients are placed in the indirect time domain, again half of the magnetization is flipped as in the phase-cycled version. The frequency in the indirect dimension can easily be determined, however the peaks have unfavorable mixed line shapes. To circumvent this problem, two transients selecting p- and n-type coherence have to be added. This leads to the same type of amplitude modulated signal as in the States method, but the $2^{½}$ intensity gain is lost (Keeler, 1985, Muhandiram, 1994 #38).

A way to work around the $2^{½}$ is by using a so-called sensitivity enhanced experiment (Cavanagh, 1991; Palmer III, 1991; Palmer III, 1992). In the indirect chemical shift dimension, the phase e.g. of the $2I_zS_y$ magnetization has a $\cos(\Omega t_1)$ dependency, and so a 90° pulse at the end of the interval t_1 flips the S_y magnetization only half the time. In total one gets an average over the cosine term, which leads to a factor $2^{½}$ loss of signal to noise that is unavoidable for all indirect dimensions that evolve chemical

shifts. The $2I_yS_z$ term created after t1 evolves into inphase proton magnetization I_x in an INEPT step and is detected subsequently, whereas the $2I_yS_x$ term is lost. The trick in sensitivity enhanced experiments is now to "park" the inphase term I_x created by the INEPT along the z-axis. At the same time the double/zero quantum term $2I_yS_x$ is converted to antiphase $2I_yS_z$ which in turn evolves into inphase I_x in a second INEPT step. Afterwards the parked I_z term is flipped to the transverse plane by a x-pulse. As a result, the total transverse magnetization present in t1 will be transferred from spins S to I (for a two spin-system IS). In a sense heteronuclear primary and stimulated echoes (Hahn, 1950) are recorded at the same time with a 90° phase difference, and unsurprisingly there is no loss in sensitivity when gradients are employed (Kay, 1992).

Another way to fully refocus the magnetization would be the application of a rf-gradient. The method of spectral editing with rf-gradients has been long recognized (Counsell, 1985). The B_1 inhomogeneity of the rf coil can be used to dephase magnetization. This method has been applied for example the suppression of zero-quantum coherences in NOESY spectra, which is not possible by pulsed field gradients or phase cycling (Mitschang, 1992). The desired magnetization is spin-locked by the rf-pulse and any component perpendicular decays.

As is the case for static pulsed field gradients, the decaying signal can be refocused by applying a gradient with opposite polarity. In such a case the phase of the signal does not depend on the position of the spins and a so-called rotary spin echo forms (Solomon, 1959). The greatest inhomogeneities of the rf field exist outside a standard coil used for high resolution NMR, where the magnetization decays approximately proportional to the inverse of the coil radius. This rf-gradient could lead to partial refocusing of prior static pulsed field gradients in z-direction (Czisch, 1996). On the other hand, static pulsed field gradients might be used to suppress B_1 inhomogeneities (Hurd, 1992). These applications all use the natural inhomogeneity of the standard coil of the spectrometer, which is not at all designed to be inhomogeneous. Another approach is to design probes, which contain an additional coil producing a linear rf-gradient (for a review see (Canet, 1997)). This rf-gradient can be used in much the same way as a static pulsed field gradient for coherence selection (Brondeau, 1992; Maas, 1993; Mutzenhardt, 1995), imaging (Hoult, 1979; Maffei, 1994; Metz, 1994) or diffusion experiments (Canet, 1997; Humbert, 1998; Kimmich, 1995; Simon, 1996).

The important point to note is that the dephasing by the rf-gradients occurs in a plane perpendicular to the effective field, e.g. the x-z plane, while static pulsed field gradients dephase in the x-y plane. In a sequence, static pulsed field gradient - $(90°)_x$-$(\text{rf-gradient})_y$, all magnetization should be refocused, if both gradients show the same positional dependence and have the same strength. Maximum sensitivity can be obtained with the combined B_0 B_1 gradient selection. The problem remains to design a probe with linear B_0 *and* B_1 gradients.

An amazingly simple way of achieving selection is to store the desired magnetization along the z-axis and apply a pulsed field gradient that purges all unwanted signals, which remained in the transverse plane. Because this method does not imply any dephasing and rephasing of the desired pathways, it is sometimes not viewed, as a "real" coherence selection by gradients, but the distinction is rather superficial. If all possible unwanted pathways are purged by a gradient, the gradient does indeed do the selection job. Examples are the application of a pulsed field gradient in the NOESY mixing time or gradients in so-called z or zz filters (Bax, 1992; John, 1992). A zz-filter can be introduced at the end of any INEPT or the beginning of a back INEPT step in a heteronuclear pulse sequence. Additional z-filters might be introduced before acquisition (Wider and Wüthrich, 1993).

In the discussion so far, all rf-pulses of the experiment have been assumed to be ideal, e.g. the desired rotation angle is expected to be the same over the whole sample volume and the whole frequency range. This is never the case in real experiments though; there will always be a number of artifacts caused by pulse imperfections. Particularly 180° pulses are sources of artifacts in spectra. An easy way to remove a bigger proportion of the imperfections of these pulses is to flank them by two pulsed field gradients of the same magnitude (Bax, 1992), a procedure which is very familiar in imaging applications, where pulse imperfections of 180° pulses are far more severe.

The main advantage of pulsed field gradients in biological applications is the very efficient water suppression. The water signal in protein samples of concentrations of 1mM or less in pure water can be reduced to be smaller than a typical signal from the protein. There are a large number of publications on this topic and the reader is referred to reviews (Aliteri, 1996; Hore, 1989). The only special water suppression technique to be mentioned here is the so-called WATER GATE. It is based on a Hahn

echo sequence with a selective pulse for the water magnetization (Liu, 1998; Piotto, 1992; Sklenar, 1993). The pulses are flanked by two identical pulsed field gradients, which refocus the desired signal and dephase the water magnetization.

2.3.2 The Design of Gradient Pulse Sequences

The general condition for the formation of a heteronuclear gradient echo has been developed in section 2.2:

The following paragraph is taken from (Thomas, 1999) which discusses the development of a computer program, based on the geometrical analysis. In the example given in (Thomas, 1999), we discuss an experiment, which produces several types of high order coherence. The experiment selects heteronuclear quadruple quantum coherence, while heteronuclear triple and double quantum coherence are suppressed.

The attenuation of a pathway depends on the vector argument, $\mathbf{k}$*, which appears as the scalar component* k_r *and* k_z *in equation (2.16).* $\mathbf{k}$ *itself depends on the inner product of the vectors* $\mathbf{p}$ *and* $\mathbf{s}$*, which is what makes it possible to interpret the mechanism of pathway selection geometrically. A pathway is rephased if* $\mathbf{k}=0$ *when field gradients are applied. In this case, the vectors* $\mathbf{s}_x$*,* $\mathbf{s}_y$ *and* $\mathbf{s}_z$ *representing the sequences of pulsed filed gradients applied along the different directions are orthogonal to the vector* $\mathbf{p}$ *representing the coherence transfer pathway. For* $\mathbf{k}$ *different from zero, i.e. if one of the vectors* $\mathbf{s}_x$*,* $\mathbf{s}_y$ *and* $\mathbf{s}_z$ *are not orthogonal to* $\mathbf{p}$*, the pathway is dephased and hence attenuated to a certain extent. Generally speaking, the larger the inner product between the pathway and the sequences of field gradients, the greater is the achievable attenuation of the signal because of the way in which Eq. (2.16) falls off.*

The overall vector space R^F *splits naturally into three parts. The first is the subspace spanned by the wanted pathways, and is hence called 'selective'. The remaining part of* R^F *is decomposed into two further parts. The suppressive subspace comprises the components of the unwanted pathways outside of the selective subspace, whilst the free subspace is any remaining part of* R^F *that can be spanned neither by wanted nor by unwanted pathways.*

The condition that a gradient sequence not perturbs the wanted signals can now be met simply by generating it from within the suppressive and free subspaces, and avoiding the selective one. The suppression of unwanted pathways depends entirely on components from the suppressive subspace. (Thomas, 1999)

In most of the pulse sequences in use for protein structure determination (Kay, 1995a; Kay, 1995b; Sattler, 1999) the situation is quite different. No higher coherence orders are excited and the number of possibilities of introducing gradients for coherence

order selection without reducing the signal to noise ratio of the experiment is very limited (Muhandiram, 1994). Usually the last back INEPT is replaced by the sensitivity-enhanced version. The two gradients inserted provide very good water-suppression and do the coherence selection (for 2 dimensions). Apart from these two gradients, a different number of additional gradients are placed around 180° Pulses and in zz-intervals (Bax, 1992). These gradients serve to suppress artifacts and prevent radiation damping of the water, in the case where water flip-back sequences are employed (Kay, 1994). The experiment is viewed as consisting of simple building blocks. The possible artifacts during such a building block are suppressed by applying pulsed field gradients in the way mentioned above. The ratio of the gradient strengths applied in different building blocks is optimized empirically, where the most crucial factor is the efficiency of the obtained water suppression. The gradient strengths are varied in non-integer ratios to avoid accidental refocusing of unwanted signals. The following discussion will show a way how this empirical procedure can be replaced by a systematic approach.

The approach is discussed on the example of the HSQC sequence with a WATERGATE (Fig. 2.1) and two zz-intervals. This relative simple pulse sequence is chosen, because the number of unwanted pathways identified by the formalism outlined below is small enough to be listed and discussed in detail within this thesis. The sensitivity enhanced version of the HSQC sequence or any other multidimensional experiment can be treated in a similar way, but the number of unwanted pathways increases relatively quickly if more free precession intervals are added.

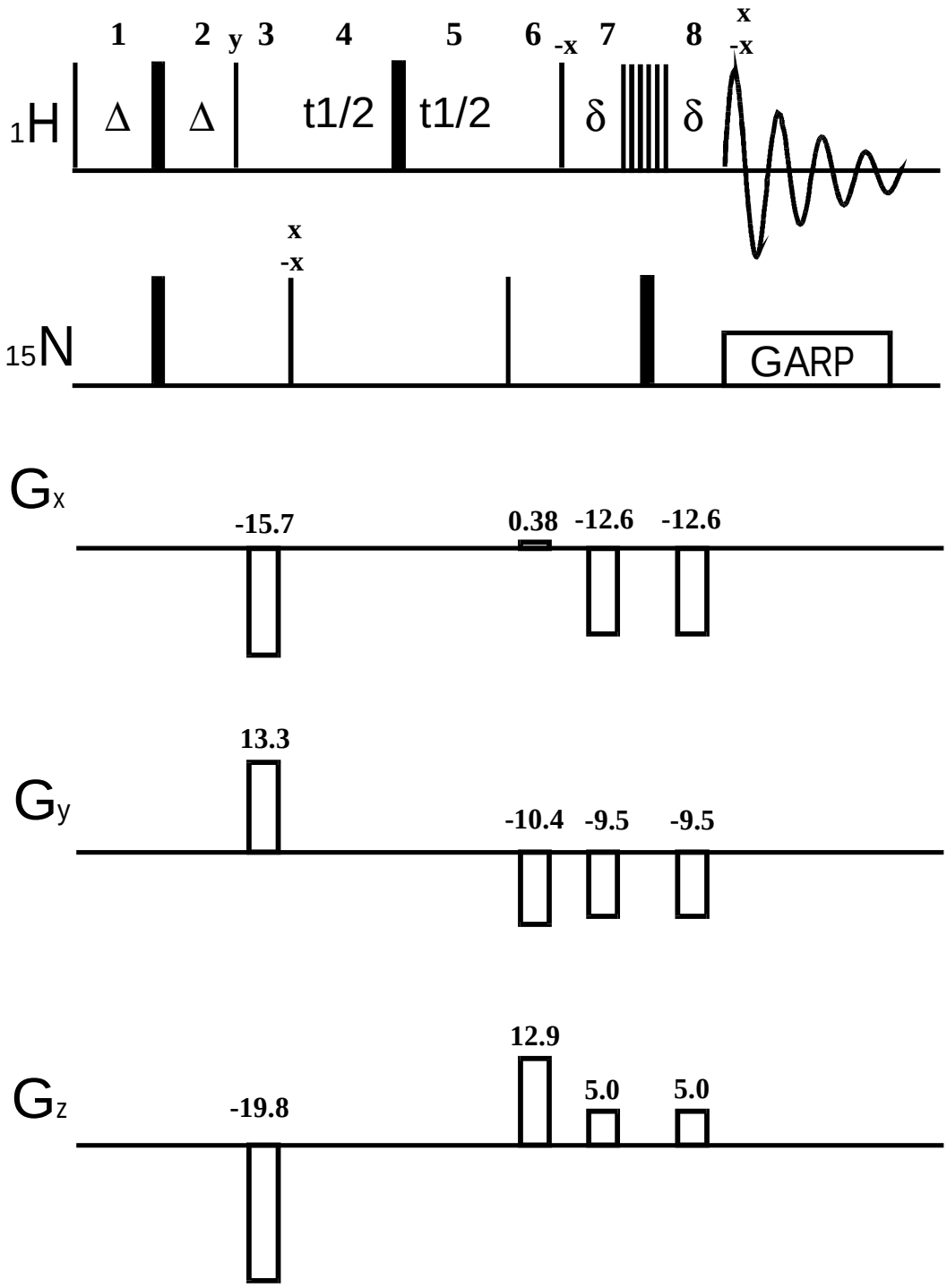

Fig. 2.1 HSQC with 3-9-19 WATERGATE and two zz-intervals. $\Delta=1/2J_{HN}$ or slightly shorter and $\delta=(2\Delta-3.37t)/2$ to compensate for J_{HN} evolution during the $(3)_x$-τ-$(9)_x$-τ-$(19)_x$-τ-$(19)_{-x}$-τ-$(9)_{-x}$-τ-$(3)_{-x}$ pulse-train. The first increment in the indirect dimension is calculated to be $(t1)_0=n/(2*SW)-[(4/\pi)*t_{\pi/2}(^{15}N)+t_{\pi}(^{1}H)]$ to calculate the phase correction in F1 or back-predict the point t1=0 (Schmieder, 1991) (n=0,1,2,.. , SW=spectral width in the ^{15}N dimension, $t_{\pi/2}(^{15}N)=90°$ Pulse length of nitrogen, $t_{\pi}(^{1}H)=180°$ Pulse length of the protons). Phase cycling: $\phi1$=x,-x,x,-x; $\phi2$=x,x,-x,-x; rec=x,-x,-x,x. Optimized gradient values are shown in lines G_x, G_y and G_z (see text).

In the HSQC experiment, the equilibrium magnetization I_z is rotated by the first 90° pulse on the protons to the transverse plane. During the first INEPT (intervals 1 and 2) antiphase proton magnetization I_yS_z builds up, which is turned into spin order I_zS_z. The first 90° pulse on ^{15}N excites antiphase nitrogen magnetization I_zS_y that evolves ^{15}N chemical shift during t1. The 180° pulse on the protons in the middle of t1 refocuses the heteronuclear coupling. At the end of t1, the magnetization is again stored as I_zS_z and finally transferred back to inphase proton magnetization, which is subsequently detected while the heteronucleus is decoupled. The pulse sequence has 8 periods of free precession in which pulsed field gradients can be placed. The coherence order of all desired pathways during these intervals are shown in Tab. 2.1.

number	1	2	3	4	5	6	7	8
1	+1	-1	0	+0.1	+0.1	0	-1	-1
2	+1	-1	0	-0.1	-0.1	0	-1	-1
3	-1	+1	0	+0.1	+0.1	0	-1	-1
4	-1	+1	0	-0.1	-0.1	0	-1	-1

Tab. 2.1 List of the four wanted coherence transfer pathways in the $^{1}H^{15}N$ HSQC experiment. The numbers in the first row refer to the intervals of free precession as shown in Fig. 2.1.

For the HSQC the origin of artifacts has been described in detail in the literature (Cavanagh, 1996; Hammarström, 1994; Shaw, 1996). Imperfections in 180° pulses including off-resonance effects and non-ideal flip angle due to rf-inhomogeneities or wrongly determined pulse-lengths are the cause of all artifacts. All of these artifacts can be analyzed in detail by a full product operator treatment. Choosing this approach gives exact results, but it requires a substantial amount of computation, especially if the pulse sequence under consideration is getting more complicated. For an efficient suppression of the resulting artifact, it should generally be enough to get an estimate of the effect of the imperfections. The effect of a pulse with flip angle Φ along the x-axis can be expressed as (Ernst, 1987)

$$I_z \xrightarrow{\Phi I_x} I_z \cos\Phi - \frac{1}{2i}\left(I^+ - I^-\right)\sin\Phi \qquad \textbf{(2.26)}$$

$$I^\pm \xrightarrow{\Phi I_x} I^\pm \cos^2\frac{\Phi}{2} + I^\mu \sin^2\frac{\Phi}{2} \pm iI_z \sin\Phi \qquad \textbf{(2.27)}$$

A pulse imperfection on a π pulse might now be written to a first approximation by replacing the ideal flip angle Φ=180° by an angle Φ=180°+ε and expanding the angular functions up to the linear term in ε:

$$I_z \xrightarrow{(\pi+\varepsilon)I_x} -I_z + 2\varepsilon\frac{1}{2i}\left(I^+ - I^-\right) + O\left(\varepsilon^2\right) \qquad \textbf{(2.28)}$$

$$I^\pm \xrightarrow{(\pi+\varepsilon)I_x} I^\mu \;\mu\; 2\varepsilon i I_z + O\left(\varepsilon^2\right) \qquad \textbf{(2.29)}$$

To be consistent in the treatment to order ε, only one 180° pulse at a time is to be imperfect. So for each wanted pathway at each of the 180° pulses in the pulse sequence, an unwanted pathway can be created by the rules given in (2.28) and (2.29), e.g. transverse magnetization is to first order flipped to the z-axis and longitudinal magnetization is converted into two transverse terms I^+ and Γ. The corresponding pathway is then evolved, with all remaining pulses treated as ideal. For the HSQC sequence this creates the following undesired pathways:

1. An imperfect 180° pulse on ^{15}N in the first INEPT creates transverse nitrogen magnetization in interval 2, doubling the number of pathways. The double and zero quantum coherences pass through to interval 3, but the 90° pulse on the protons creates single quantum ^{15}N magnetization as well. Each pathways splits into three new pathways. The following 90° pulse on nitrogen creates transverse and longitudinal ^{15}N terms, splitting all pathways again into three pathways. The 180° pulse on the protons does not create any new pathways. Of the terms created by the second 90° pulse on nitrogen, only the ones with longitudinal nitrogen lead to a detectable signal. Since only –1 proton magnetization is detected by convention (see e.g. (Kessler, 1988)), only terms with +1 need to be considered in interval 7. Thus the imperfections of the first 180° pulse on ^{15}N lead to a total of 36 unwanted pathways listed in Previous page: Tab. 2.2 (# 1-36).
2. The 180° pulse on the protons during the first INEPT creates to first order longitudinal proton magnetization. The further evolution leads to 12 additional unwanted pathways listed in Previous page: Tab. 2.2 (# 37-48).
3. Imperfections of the 180° pulse in the indirect evolution time create zero and double quantum coherences in interval 5. A total of 8 additional unwanted pathways are created (Previous page: Tab. 2.2 #49-56).
4. The last 180° pulse on nitrogen is going to create unobservable double and zero quantum coherences in the ideal pathway. However, the double and zero quantum coherences created by the last 90° pulse on nitrogen are turned into observable proton magnetization. Another 8 unwanted pathways are added (Previous page: Tab. 2.2 # 57-64)
5. Finally, the last 180° rotation on the protein signal by the WATERGATE pulse has to be analyzed. It is going to create longitudinal magnetization of each transverse proton term to a first approximation. This is not observable, and so no additional terms are added at this point.

	1	2	3	4	5	6	7	8
1	+1	-0.9	+1.1	+1.1	-0.9	-1	+1	-1
2	+1	-0.9	+1.1	+1	-1	-1	+1	-1
3	+1	-0.9	+1.1	+0.9	-1.1	-1	+1	-1
4	+1	-0.9	+0.1	+0.1	0.1	0	+1	-1
5	+1	-0.9	+0.1	0	0	0	+1	-1
6	+1	-0.9	+0.1	-0.1	-0.1	0	+1	-1
7	+1	-0.9	-0.9	-0.9	+1.1	+1	+1	-1
8	+1	-0.9	-0.9	-1	+1	+1	+1	-1
9	+1	-0.9	-0.9	-1.1	+0.9	+1	+1	-1
10	+1	-1.1	+0.9	+1.1	-0.9	-1	+1	-1
11	+1	-1.1	+0.9	+1	-1	-1	+1	-1
12	+1	-1.1	+0.9	+0.9	-1.1	-1	+1	-1
13	+1	-1.1	-0.1	+0.1	0.1	0	+1	-1
14	+1	-1.1	-0.1	0	0	0	+1	-1
15	+1	-1.1	-0.1	-0.1	-0.1	0	+1	-1
16	+1	-1.1	-1.1	-0.9	+1.1	+1	+1	-1
17	+1	-1.1	-1.1	-1	+1	+1	+1	-1
18	+1	-1.1	-1.1	-1.1	+0.9	+1	+1	-1
19	-1	+1.1	+1.1	+1.1	-0.9	-1	+1	-1
20	-1	+1.1	+1.1	+1	-1	-1	+1	-1
21	-1	+1.1	+1.1	+0.9	-1.1	-1	+1	-1
22	-1	+1.1	+0.1	+0.1	0.1	0	+1	-1
23	-1	+1.1	+0.1	0	0	0	+1	-1
24	-1	+1.1	+0.1	-0.1	-0.1	0	+1	-1
25	-1	+1.1	-0.9	-0.9	+1.1	+1	+1	-1
26	-1	+1.1	-0.9	-1	+1	+1	+1	-1
27	-1	+1.1	-0.9	-1.1	+0.9	+1	+1	-1
28	-1	+0.9	+0.9	+1.1	-0.9	-1	+1	-1
29	-1	+0.9	+0.9	+1	-1	-1	+1	-1
30	-1	+0.9	+0.9	+0.9	-1.1	-1	+1	-1
31	-1	+0.9	-0.1	+0.1	0.1	0	+1	-1
32	-1	+0.9	-0.1	0	0	0	+1	-1
33	-1	+0.9	-0.1	-0.1	-0.1	0	+1	-1
34	-1	+0.9	-1.1	-0.9	+1.1	+1	+1	-1
35	-1	+0.9	-1.1	-1	+1	+1	+1	-1
36	-1	+0.9	-1.1	-1.1	+0.9	+1	+1	-1
37	+1	0	+1	+1.1	-0.9	-1	+1	-1
38	+1	0	+1	+1	-1	-1	+1	-1
39	+1	0	+1	+0.9	-1.1	-1	+1	-1
40	+1	0	-1	-0.9	+1.1	+1	+1	-1
41	+1	0	-1	-1	+1	+1	+1	-1
42	+1	0	-1	-1.1	+0.9	+1	+1	-1
43	-1	0	+1	+1.1	-0.9	-1	+1	-1
44	-1	0	+1	+1	-1	-1	+1	-1
45	-1	0	+1	+0.9	-1.1	-1	+1	-1
46	-1	0	-1	-0.9	+1.1	+1	+1	-1
47	-1	0	-1	-1	+1	+1	+1	-1
48	-1	0	-1	-1.1	+0.9	+1	+1	-1
49	+1	-1	0	+0.1	+1.1	+1	+1	-1
50	+1	-1	0	+0.1	-0.9	-1	+1	-1
51	+1	-1	0	-0.1	+0.9	+1	+1	-1
52	+1	-1	0	-0.1	-1.1	-1	+1	-1
53	-1	+1	0	+0.1	+1.1	+1	+1	-1
54	-1	+1	0	+0.1	-0.9	-1	+1	-1
55	-1	+1	0	-0.1	+0.9	+1	+1	-1
56	-1	+1	0	-0.1	-1.1	-1	+1	-1
57	+1	-1	0	+0.1	+0.1	+0.1	+1.1	-1
58	+1	-1	0	+0.1	+0.1	-0.1	+0.9	-1
59	+1	-1	0	-0.1	-0.1	+0.1	+1.1	-1
60	+1	-1	0	-0.1	-0.1	-0.1	+0.9	-1
61	-1	+1	0	+0.1	+0.1	+0.1	+1.1	-1
62	-1	+1	0	+0.1	+0.1	-0.1	+0.9	-1
63	-1	+1	0	-0.1	-0.1	+0.1	+1.1	-1
64	-1	+1	0	-0.1	-0.1	-0.1	+0.9	-1

Previous page: Tab. 2.2 Pathways created in first order approximation by imperfect 180° pulses.

All in all there are 64 unwanted pathways having arisen from pulse imperfections on the 180° pulses. In the evolution of the coherence orders an *ideal heteronuclear NH two spin system* was assumed. Additionally, it is important to take any proton into account, which is not coupled to ^{15}N. Here especially the water magnetization is important. Because of the large magnitude of the water magnetization, it was found to be necessary to include pulse imperfections on all proton pulses in creating the unwanted pathways arising from water magnetization. With the same approximation as above for 180° pulses, the following relations to first order in pulse imperfections for 90° pulses hold:

$$I_z \xrightarrow{\left(\frac{\pi}{2}+\varepsilon\right)I_x} -\frac{1}{2i}\left(I^+ - I^-\right) - \varepsilon I_z + O\left(\varepsilon^2\right) \qquad \textbf{(2.30)}$$

$$I^\pm \xrightarrow{\left(\frac{\pi}{2}+\varepsilon\right)I_x} \frac{1}{2}I^\pm(1-\varepsilon) + \frac{1}{2}I^\mu(1-\varepsilon) \pm iI_z + O\left(\varepsilon^2\right) \qquad \textbf{(2.31)}$$

The unwanted pathways arising from water magnetization are treated in the same way as the pulse imperfection pathways above. The "ideal" water-pathway, e.g. the water-pathway with all pulse flip-angles taken to be exactly equal to their nominal value, is going to be written down first. Then flip angle deviations to first order of all proton pulses are considered. Again, only one pulse at a time is going to be treated as imperfect, whereas at the same time all other pulses are considered as being perfect. It should be pointed out that some of the neglected higher order terms for the water pathways are probably bigger than the first order protein terms considered above. However, we found that including these terms does not improve the water suppression, because the residual water observed experimentally is due to other factors.

Protons not coupled to ^{15}N, which show no homonuclear proton-proton coupling, are flipped to the –y-axis by the first $(90°)_x$ pulse. The second 90° pulse on the protons is applied along the y-axis, so the magnetization stays in the transverse plane during the two zz-intervals and the indirect evolution period t1. The last $(90°)_x$ is going to flip

the magnetization back to the z-axis. This "ideal" water pathway does not contribute to the observed signal.

The first order treatment results in the following unwanted pathways:

1. Imperfections in the first 90° pulse of the experiment will leave some magnetization along the z-axis. This magnetization is getting transverse in interval 3 and will lead to observable magnetization. The WATER GATE pulse is going to rotate the water magnetization by 360°, resulting in pathways # 65 and # 66 of Tab. 2.3.
2. The first 180° pulse of the experiment flips the water back to the z-axis. This creates the 4 unwanted pathways (Tab. 2.3 # 67-70).
3. If the second 90° pulse is not perfect, the water is rotated to the z-axis during the indirect evolution period (Tab. 2.3 pathways # 71, 72).
4. Imperfection of the other proton pulses excite pathways # 73-76 (180° pulse during t1), # 77-80 (90° pulse after t1) and # 81-84 (WATER GATE pulse).

	1	2	3	4	5	6	7	8
65	0	0	+1	+1	-1	-1	-1	-1
66	0	0	-1	-1	+1	+1	-1	-1
67	+1	0	+1	+1	-1	-1	-1	-1
68	+1	0	-1	-1	+1	+1	-1	-1
69	-1	0	+1	+1	-1	-1	-1	-1
70	-1	0	-1	-1	+1	+1	-1	-1
71	+1	-1	0	0	0	0	-1	-1
72	+1	-1	0	0	0	0	-1	-1
73	+1	-1	+1	+1	0	0	-1	-1
74	+1	-1	-1	-1	0	0	-1	-1
75	-1	+1	+1	+1	0	0	-1	-1
76	-1	+1	-1	-1	0	0	-1	-1
77	+1	-1	+1	+1	-1	-1	-1	-1
78	+1	-1	-1	-1	+1	+1	-1	-1
79	-1	+1	+1	+1	-1	-1	-1	-1
80	-1	+1	-1	-1	+1	+1	-1	-1
81	+1	-1	+1	+1	-1	-1	0	-1
82	+1	-1	-1	-1	+1	+1	0	-1
83	-1	+1	+1	+1	-1	-1	0	-1
84	-1	+1	-1	-1	+1	+1	0	-1

Tab. 2.3 Coherence transfer pathways of the water magnetization, excited by pulse imperfection in the HSQC experiment (Fig. 2.1).

So in total there are 20 additional unwanted pathways from water proton magnetization and the input file for TRIPLE GRADIENT or Z GRADIENT consists of 4 wanted and 84 unwanted pathways.

The program TRIPLE GRADIENT and its one-dimensional analogue Z GRADIENT allow the specification of a weight factor for each individual unwanted coherence transfer pathway. This option is used to reflect different signal amplitudes for the unwanted pathways, which is especially useful in the case of strong solvent signals. In a typical protein NMR experiment, the sample concentration is in the millimolar

range, while the water concentration is in the molar range. The water signal is therefore 1000 to 10000 times stronger than any protein signal. Therefore an optimized gradient sequence should suppress the unwanted water pathways more efficiently.

Having decided which are the wanted and unwanted pathways, the free evolution periods during which a gradient might be applied have to be specified in the input file for the GRADIENT programs. Since in the present example we want to retain all wanted pathways, there is no possibility to apply any effective gradient during the indirect evolution time. If gradients are allowed during intervals 4 and 5 (Fig. 2.1), the effect of the gradient in interval 5 refocuses the effect of the gradient in interval 4. Since the wanted pathways have the same coherence order in intervals 4 and 5, the two gradients are of the same amplitude, but have opposite sign.

Allowing gradients during intervals 3, 6, 7 and 8 leads to the suppression of all unwanted pathways. Choosing less than four intervals results in the refocusing of some unwanted pathways. The following discussion will focus on the results of different optimization runs of TRIPLE GRADIENT and Z GRADIENT allowing gradients during intervals 3, 6, 7 and 8 with different relative weights given to the protein and the water pathways. The duration of each gradient is set to 1 ms.

After reading the input file, both programs calculate the selective, suppressive and free subspaces by repeated application of the *Gram-Schmidt* procedure. The first represents the subspace spanned by the wanted pathways, the second the subspace spanned by the unwanted, whilst the free subspace is any remaining part of R^F that can be spanned neither by a wanted nor by an unwanted pathway. The condition that a gradient sequence not perturbs the wanted signals can now be met simply by generating it from within the suppressive and free subspaces. Details of the computation are given in (Thomas, 1999).

In our example, we choose four intervals, so we are operating in R^4. One basis vector represents the wanted pathways and three orthogonal basis vectors represent the unwanted pathways. The free subspace is empty. The orthonormal vectors constructed by the *Gram-Schmidt* procedure are listed in Tab. 2.4. The three orthonormal base vectors of the suppressive subspace are named **A**, **B** and **C**. The coherence order of the

wanted pathways during the zz-intervals is zero, so the vector representing the selective subspace has zero components in the intervals 3 and 6.

	free precession interval			
	3	6	7	8
	vector representing desired pathways			
	0.00	0.00	0.71	-0.71
	orthogonal vectors representing unwanted pathways			
A	0.74	-0.67	0.00	0.00
B	0.67	0.74	0.00	0.00
C	0.00	0.00	0.71	0.71

Tab. 2.4 Components of the base vectors of the selective and suppressive subspace in the four selected intervals of the HSQC sequence of Fig. 2.1.

The components of all unwanted pathways in the suppressive subspace can now be expressed as a linear combination of vectors **A**, **B** and **C** (**x** = a***A**+b***B**+c***C**). The expansion coefficients for all unwanted pathways are listed in Tab. 2.5. Only 19 independent vectors representing the unwanted pathways remain, if only those 4 intervals of free precession are chosen. The unwanted protein pathways are almost restricted to the plane spanned by **A** and **B**, with the only exception of group 11 and 12 having a small component c. The corresponding pathways 57-64 are excited by imperfections of the last 180° pulse on nitrogen (Previous page: Tab. 2.2).

Number	group	a	B	c
1-3. 19-21	1	1.49	0.00	0.00
16-18. 34-36	2	-1.49	0.00	0.00
37-39. 43-45	3	1.41	-0.07	0.00
40-42. 46-48	4	-1.41	0.07	0.00
10-12. 28-30	5	1.34	-0.13	0.00
7-9. 25-27	6	-1.34	0.13	0.00
50. 52. 54. 56	7	0.67	-0.74	0.00
49. 51. 53. 55	8	-0.67	0.74	0.00
4-6. 22-24	9	0.07	0.07	0.00
13-15. 31-33	10	-0.07	-0.07	0.00
58. 60. 62. 64	11	0.07	-0.07	-0.07
57. 59. 61. 63	12	-0.07	0.07	0.07
65. 67. 69. 77. 79	13	1.41	-0.07	-1.41
66. 68. 70. 78. 80	14	-1.41	0.07	-1.41
81. 83	15	1.41	-0.07	-0.71
82. 84	16	-1.41	0.07	-0.71
73. 75	17	0.74	0.67	-1.41
74. 76	18	-0.74	-0.67	-1.41
71. 72	19	0.00	0.00	-1.41

Tab. 2.5 Components a, b and c of the unwanted pathways in the base A, B, C. The numbers in the first column correspond to the numbers of the unwanted pathways in Tab. 2-11. Identical weight factors have been given to all pathways.

The relative weight of all pathways listed in Tab. 2.5 is equal to 1. The different magnitudes of the vectors are mainly caused by their different magnitude of coherence order during the zz-intervals. The weight factor just multiplies all components by a constant specified for each pathway. The dependency of the optimized gradient sequence for a one-dimensional gradient sequence on the weight factor for the water pathways can be anticipated: The solution will be more and more driven to point along base-vector **C**. The results of calculations using Z GRADIENT is summarized in Tab. 2.7.

weights on water pathways	#	gradient strengths				projection of gradients		
		3	6	7	8	a	b	c
0	1	43.85	-40.03	-32.15	-32.15	0.63	0.00	-0.37
1	2	43.18	-40.39	-29.76	-29.76	0.66	0.00	-0.34
1000	3	13.04	7.32	36.96	36.96	0.01	0.07	0.92
1000. 2000	4	10.90	6.21	37.10	37.10	0.01	0.05	0.95
10000	5	-6.12	-3.44	-36.78	-36.78	0.00	-0.02	-0.98
10000000	6	-0.62	-0.35	36.73	36.73	0.00	0.00	1.00
only water	7	0.00	0.00	-36.73	-36.73	0.00	0.00	-1.00

Tab. 2.6 Optimized z-gradients sequences for the HSQCzz-wg sequence (Fig. 2.1) calculated with Z-GRADIENT. The gradients strengths are listed in [ms*G/cm]. The normalized projections along the base-vectors A B and C are listed in the last three columns.

Having gradients around the WATERGATE pulse only optimizes water suppression. In the base **A**, **B**, **C** this corresponds to applying a gradient in the direction of **C** only. Any additional gradient component in the plane spanned by **A** and **B** will result in an optimized suppression of the even numbered groups and lesser suppression of the odd numbered groups of Tab. 2.5 and vice versa.

A three dimensional suppressive subspace is obviously very well suited for application of gradients in three dimensions. The optimized gradient sequences for a three-gradient system are listed in Tab. 2.7.

weights on water paths	#	axis	gradient strengths 3	6	7	8	projection of gradients a	b	c
0	1	x	-36,88	26,92	19,03	19,03	-0,73	-0,01	0,26
		y	-36,88	26,92	19,03	19,03	-0,73	-0,01	0,26
		z	-38,37	28,91	21,29	21,29	-0,71	-0,01	0,28
1	2	x	-35,79	-25,61	-18,16	-18,16	-0,03	-0,71	-0,25
		y	35,80	-25,88	-17,66	-17,66	0,75	0,01	-0,24
		z	37,28	-27,73	-20,99	-20,99	0,70	0,01	-0,29
1000	3	x	-15,72	0,38	-12,59	-12,59	-0,25	-0,19	-0,56
		y	13,27	-10,49	-9,53	-9,53	0,61	0,00	-0,39
		z	-19,78	12,85	5,02	5,02	-0,89	-0,02	0,08
1000, 2000	4	x	-14,74	2,30	-11,94	-11,94	-0,31	-0,13	-0,56
		y	-12,26	10,02	9,73	9,73	-0,57	0,00	0,43
		z	19,25	-12,17	-4,18	-4,18	0,91	0,03	-0,06
10000	5	x	13,01	-9,12	-9,34	-9,34	0,58	0,01	-0,41
		y	-12,57	7,80	-7,90	-7,90	-0,62	-0,02	-0,36
		z	6,73	4,24	14,47	14,47	0,01	0,12	0,87
10000000	6	x	-10,09	8,73	9,25	9,25	-0,51	0,00	0,49
		y	9,98	-8,67	9,15	9,15	0,51	0,00	0,49
		z	-0,75	-0,46	-14,41	-14,41	0,00	0,00	-1,00
only water	7	x	9,98	-8,71	9,21	9,21	0,51	0,00	0,49
		y	9,98	-8,71	-9,21	-9,21	0,51	0,00	-0,49
		z	0,00	0,00	14,41	14,41	0,00	0,00	1,00

Tab. 2.7 Optimized x-, y- and z-gradient sequences for the HSQCzz-wg sequence (Fig. 2.1) calculated with TRIPLE GRADIENT. The gradients strengths are listed in [ms*G/cm]. The normalized projections along the base-vectors A B and C are listed in the last three columns.

Selecting the protein pathways only results in the same gradient sequence in all three dimensions. The small differences in the magnitude of the transverse and z gradients are due to the different envelope functions reflecting the sample shape (see Figs. 5, 6 and 7 in (Thomas, 1999)).

If only the water pathways are selected, the z-gradient sequence corresponds to gradients placed around the WATER GATE pulse only. The x- and y-gradients are pointing in opposite directions in the a-c plane. The component of the gradient sequence along vector B is only different from 0 for intermediate weights of the water pathways.

The result of the optimization in three dimensions is not as obvious as in the one-dimensional case. For more complicated pulse sequences with a larger suppressive subspace, a direct visualization of the unwanted vectors is impossible. However, the programs TRIPLE GRADIENT and Z GRADIENT are an efficient tool to find an optimal gradient sequence in these cases as well.

The experimental water suppression of the calculated z-gradient and triple-gradients sequences are shown in Fig. 2.2 and

Fig. 2.3. To avoid any effects from the phase cycling or partial saturation of the water resonance during the pulse sequence, only one scan with the indirect chemical shift dimension set to 3 μs, and no preceding dummy scan is shown. Any effects resulting from the phase cycling or partial saturation of the water resonance during the pulse sequence are therefore avoided and the efficiency of the water suppression of the gradient sequence alone is monitored. The receiver gain was set to 512 for all experiments. Gradients were applied with the shape of a half sine wave with the gradient strength in percent of the maximum gradient strength as specified in Tab. 2.6 and Tab. 2.7. The first 1k points are recorded with a dwell time of 60 μs corresponding to a total acquisition time of 61.44ms. This corresponds to a typical acquisition time for protons in an experiment with ^{15}N decoupling. The experiments show that the water suppression is sufficiently good to allow a receiver gain of 512. However, the theoretically predicted improvement of the gradient sequences with respect to water suppression could not be confirmed.

The difference between calculated and observed water suppression rates is caused mainly by radiation damping of the water signal (caused by the coupling of the rf-circuit to the very strong water signal). The influence of radiation damping is seen more clearly by looking at the full FID of the water signal, e.g. extending the acquisition time to around 2s and changing the phase of the 90° proton pulse before the second zz-interval to x. This results for example in an almost full recovery of the water magnetization in trace 7 Fig. 2.1 of the z-gradient experiment with water-gate gradients only. In this case, the water magnetization is flipped to the negative z-axis by the last proton 90° pulse, where it stays until the acquisition is started. During the acquisition period, the water is then brought to the transverse plane and back to the +z axis by radiation damping.

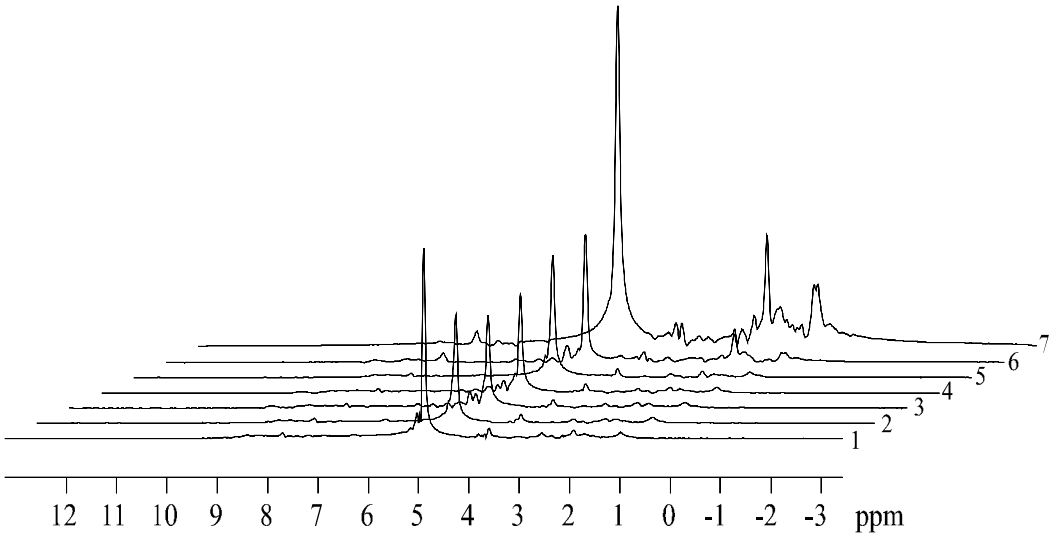

Fig. 2.2 Comparison of the water suppression for different settings of the z-gradient strengths in the HSQC sequence of Fig. 2.1. The number on the right side of each trace corresponds to the number in column # of Tab. 2.6.

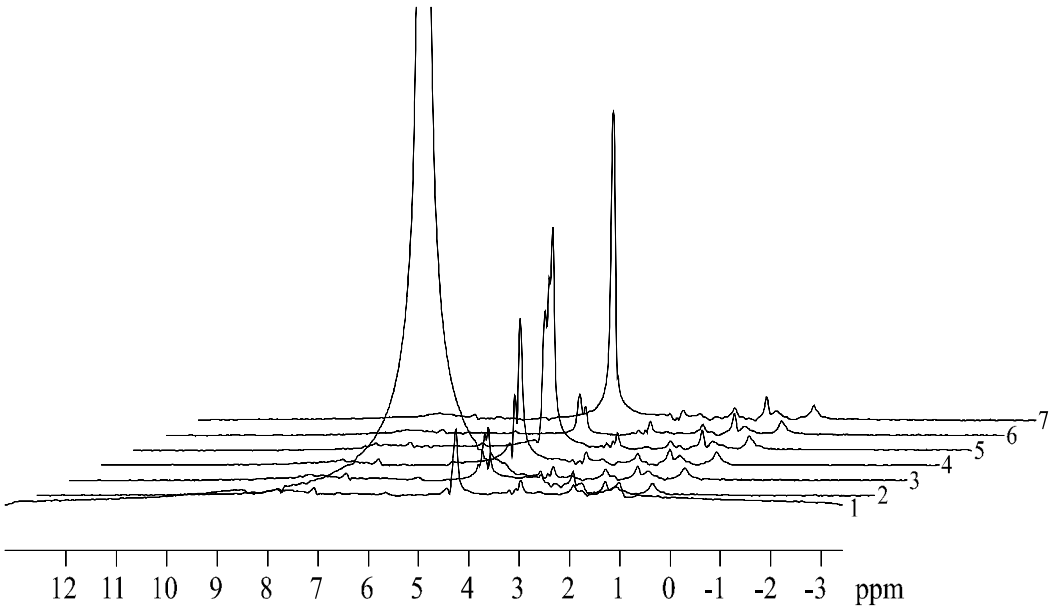

Fig. 2.3 Comparison of the water suppression for different settings of the x-, y- and z-gradient strengths in the HSQC sequence of Fig. 2.1. The number on the right side of each trace corresponds to the number in column # of Tab. 2.7.

If a number of dummy scans is applied before the data acquisition and the two step phase cycle to select for ^{15}N bound protons, the water suppression is found to be very good for all of the calculated sequences. This means, that specifying the unwanted

pathways in the way introduced above leads to good water suppression almost independent of the weight factors. Two spectra recorded with the optimized z-gradients (Fig. 2.4) and triple-gradients (Fig. 2.5) show the efficiency of the water gradient sequences. The spectra are recorded with four scans per t1 increment with a relaxation delay of 1s between the scans on a 0.8 mM sample of the HRDC domain (Liu, 1999) (80 amino acids). 256 indirect time increments were recorded in 19 minutes. The spectra have been multiplied with the decaying quarter of a squared sine function in both dimensions and zero filled to a 2k x 1k data matrix prior to Fourier transform. Both spectra are plotted on equal intensity contour levels. In addition, the positive projection of all rows of the two-dimensional spectrum is shown on top of the contour plot.

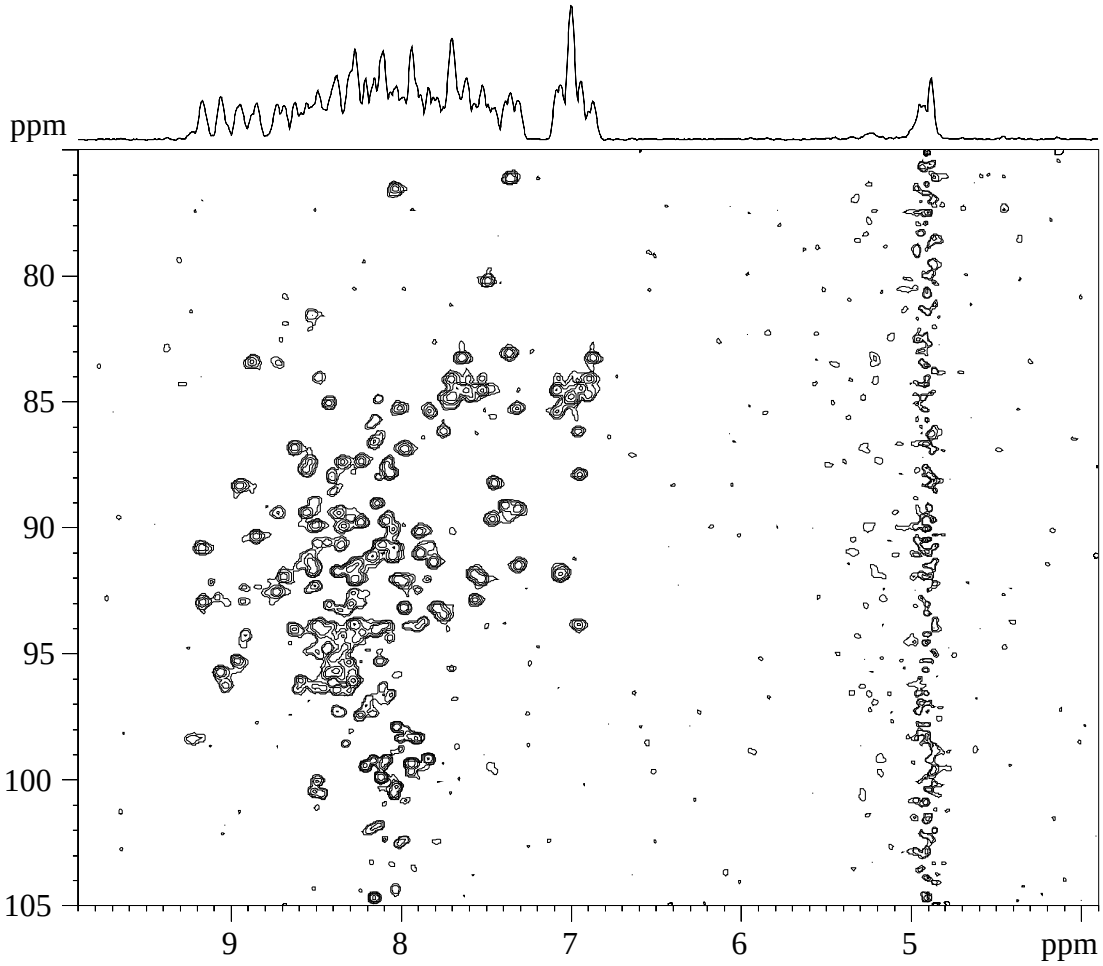

Fig. 2.4 ^{1}H-^{15}N HSQC spectrum of a 0.8 mM protein sample in H_2O recorded with the pulse-sequence of Fig. 2.1. The spectrum was recorded with 4 scans for each t1 increment and a recycle delay of 1s. The z-gradient strength in % was set to 13.04, 7.32, 36.96 and 36.96 for the four gradients.

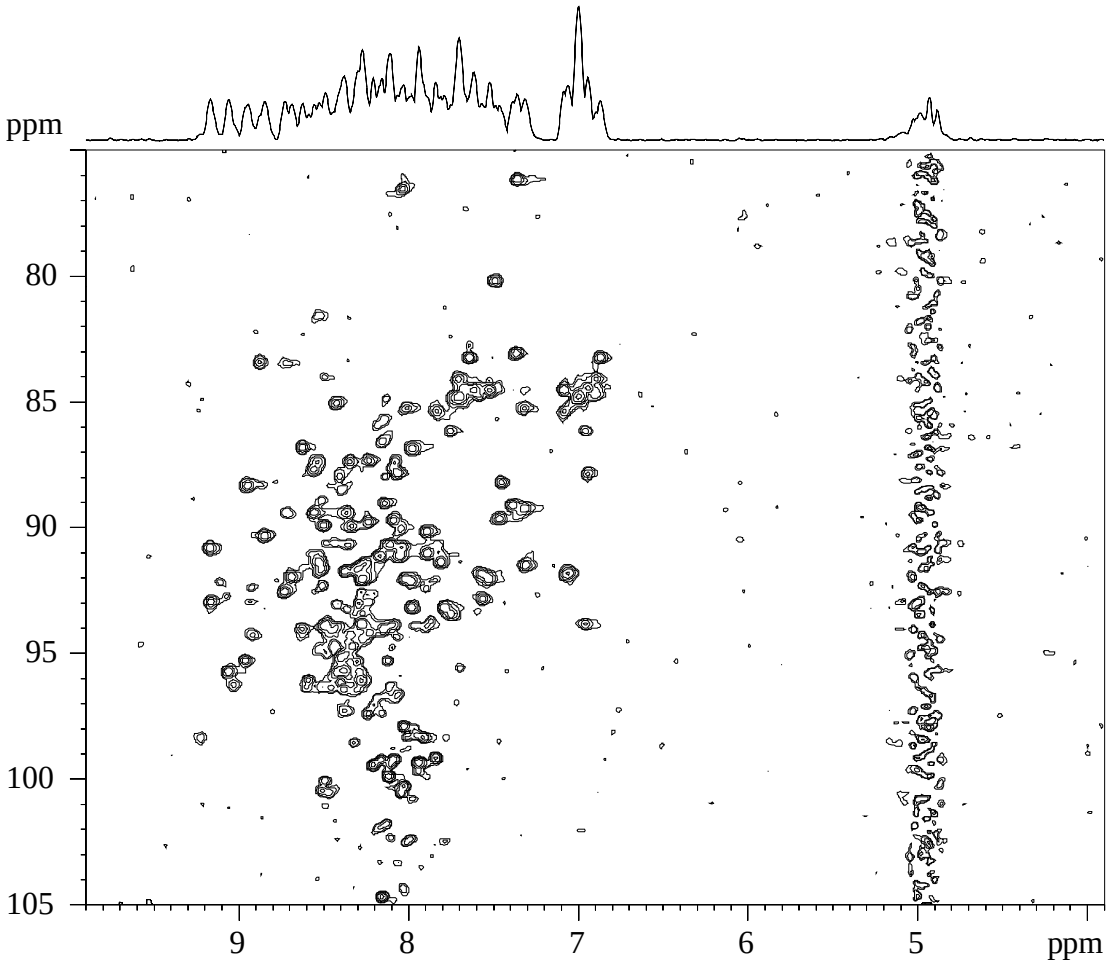

Fig. 2.5 ^{1}H-^{15}N HSQC spectrum of a 0.8 mM protein sample in H_2O recorded with the pulse-sequence of Fig. 2.1. The spectrum was recorded with 4 scans for each t1 increment and a recycle delay of 1s. The x-, y- and z-gradient values are as indicated in Fig. 2.1.

The ratio of the integral from 9.5 to 6 ppm to the integral from 5.5 to 4.5 ppm is 100:10 for the z-gradient and 100:9 for the triple-gradient version. Thus, the triple-gradient version performs only slightly better than the z-gradient, although the water suppression in the single scan experiments of Fig. 2.2 and Fig. 2.3 is showing an approximately three times better water suppression for the triple-gradient experiment. (This can be seen by overlaying one of the 1D traces of Fig. 2.2 and Fig. 2.3, which are **not** plotted with the same intensity scale). A possible explanation is that the additional two-step phase cycle on the ^{15}N 90° pulse is more efficient for additional water-suppression in the z-axis version than in the triple-axis version. The active shielding of the z-gradient coil is more efficient compared to the transverse gradient coils on the probehead used for the experiments. This causes a higher reproducibility

of the water signal in different scans of the z-gradient version and thus a more efficient cancellation of the water resonance by subtraction of alternate scans in the acquisition buffer. Trial and error optimizations of the gradient sequences by an experienced user performed typically about 5 % worse giving an intensity ratio of the integrated signal to the water in the positive projection of 100:15.

These experiments show that the above treatment of the water-signal in the development of sequences of pulsed field gradients leads to satisfactory water-suppression and artifact reduction. A rather simple example of the four gradients in the HSQC water-gate sequence is chosen because it allows a relative nice pictorial representation of the calculated gradient sequences in terms of the geometric approach.

It was found to be important to treat possible pulse imperfections in a consistent way – especially for the strong water signal. With the approach outlined in this section, a simple and straightforward way of dealing with imperfections is being presented. The approach depicted here is expected to work well, if unwanted signals arise from pulse imperfections only. Any considerations concerning different spin systems and coupling patterns have been discarded for simplicity. Any unwanted signals arising from different spin topologies should be identified via a product operator analysis. In the case of protein NMR this is usually straight forward, since the coupling patterns and chemical shift ranges for the 20 amino acids are very well known. In cases where unwanted signal intensities arising from different spin systems have equal or higher intensities as the wanted signals, pulse imperfections for these "ideal" unwanted pathways can be treated accordingly.

In a more general approach all possible pathways that could be created by any spin system would have to be considered. This would create a large number of pathways – for example there are 151,875 pathways reported in the case of a HSQC sequence (Jerschow, 1998). Such a large number of unwanted pathways are difficult to handle by TRIPLE GRADIENT or Z GRADIENT, even if many pathways could be rejected as redundant for a limited selection of intervals during which pulsed field gradients were to be applied. The main advantage of doing a selection of unwanted pathways is that the optimized gradient sequence suppresses those especially well. Adding more pathways, which do not contribute significantly to the detected signal, might result in

a gradient sequence, which would not be as efficient in suppressing the strong unwanted signals.

The selection of significant unwanted pathways could be done automatically by using the approach outlined in (Jerschow, 1998). If a pulse sequence without any gradients is given to the program outlined by Jerschow and Müller, the most significant remaining pathways and their transfer amplitudes are returned and could be fed directly into the gradient optimization of TRIPLE GRADIENT or Z GRADIENT. This approach is also expected to be very robust. However, neglecting any transfer amplitudes by not using any information about the spin topology as done in the approach of (Jerschow, 1998) might again lead to the inclusion of unwanted pathway with negligible contributions. On the other hand, a full automation of the selection of unwanted pathways reduces the problem to a purely technical one.

Having artifact free spectra is especially important in cases where quantitative measurements are to be performed. The identification of artifacts in HSQC spectra and their removal was done during the setup of experiments for an investigation of the dynamics of the PH domain of β-spectrin (Gryk, 1998). The changes of the internal dynamics of the PH domain by ligand binding are very subtle and we found that high quality spectra were a prerequisite for their observation.

2.4 Diffusion in multi-pulse heteronuclear experiments

2.4.1 General expressions for the signal attenuation by rectangular and sine shaped gradients

In section 2.2 we get two general expressions (Eqs. (2.24) and (2.25)) for the influence of diffusion on the attenuation of a coherence order transfer pathway. This chapter is going to give some specific solutions to these equations. The equation in the time domain (2.25) is more straightforward to solve directly without any assumptions about the gradient pulse sequence. The integral is split into F integrals over the time intervals Δ_i between the end point of two consecutive pulsed field gradients (see Fig. 2.6). The coherence order does not change during each of the gradients and two consecutive gradients are separated by one or more rf-pulses. The gradient shapes are specified explicitly by the shape factors f_α^i. The shape factors considered are

rectangular and the first half of a sine wave, which are the shape factors most widely used in high resolution experiments.

Rectangular gradients

First we are going to treat the case of rectangular gradients with the same shape f for the three Cartesian dimensions α, e.g.

$$f_\alpha^i(t) = f(t) = \begin{cases} 1 & \tau_i - \delta_i \le t \le \tau_i \\ 0 & otherwise \end{cases} \qquad \textbf{(2.32)}$$

A schematic figure of the sequence of pulsed field gradient is given in Fig. 2.6

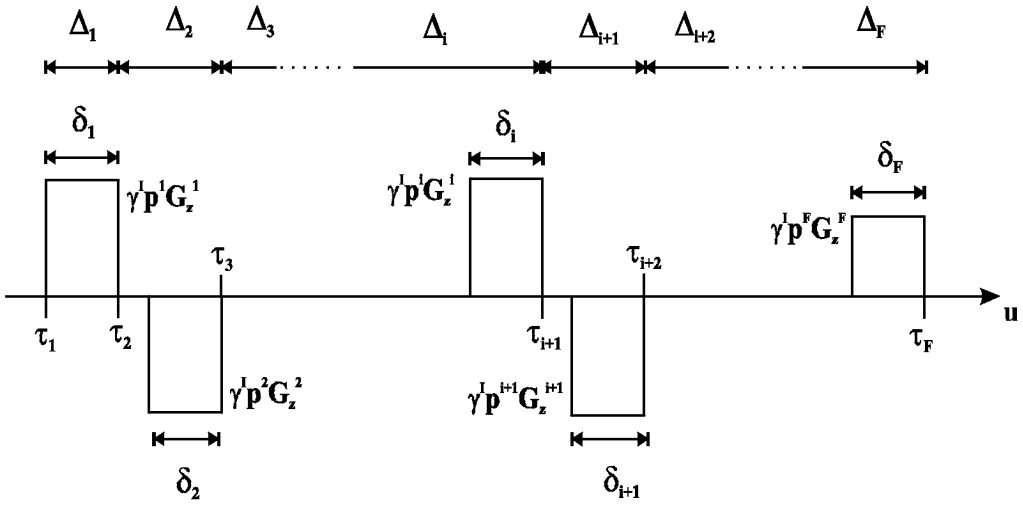

Fig. 2.6 Schematic representation of a series of rectangular pulsed field gradients. Between the end of one gradient and the beginning of the next, one or a series of rf-pulses is applied, which lead to changes in the coherence order p^i.

The solution of (2.25) during the time interval Δ_i divides into two parts: the time δ_i with the effective gradient of $G^i p^i$ is on and the remaining time with zero gradient. The first part gives:

$$\int_{\tau_i-\delta_i}^{\tau_i}\left|\gamma_I\left(\sum_{j=1}^{i-1}p^j s_\alpha^j + p^i G_\alpha^i \int_{\tau_i-\delta_i}^{u} dt'\right)\right|^2 du$$

$$= \gamma_I{}^2 \int_{\tau_i-\delta_i}^{\tau_i}\left|\left(\mathbf{p}^{i-1}\mathbf{s}_\alpha^{i-1} + p^i G_\alpha^i\left(u-(\tau_i-\delta_i)\right)\right)\right|^2 du$$

$$= \gamma_I{}^2 \int_{\tau_i-\delta_i}^{\tau_i}\left(\left(\mathbf{p}^{i-1}\mathbf{s}_\alpha^{i-1}\right)^2 + 2\mathbf{p}^{i-1}\mathbf{s}_\alpha^{i-1}p^i G_\alpha^i\left(u-(\tau_i-\delta_i)\right) + \left(p^i G_\alpha^i\left(u-(\tau_i-\delta_i)\right)\right)^2\right)du$$

$$= \gamma_I{}^2\left(\left(\mathbf{p}^{i-1}\mathbf{s}_\alpha^{i-1}\right)^2(u) + 2\mathbf{p}^{i-1}\mathbf{s}_\alpha^{i-1}p^i G_\alpha^i\frac{\left(u-(\tau_i-\delta_i)\right)^2}{2} + \left(p^i G_\alpha^i\right)^2\frac{\left(u-(\tau_i-\delta_i)\right)^3}{3}\Bigg|_{\tau_i-\delta_i}^{\tau_i}\right)$$

$$= \gamma_I{}^2\left(\left(\mathbf{p}^{i-1}\mathbf{s}_\alpha^{i-1}\right)^2\delta_i + \mathbf{p}^{i-1}\mathbf{s}_\alpha^{i-1}p^i G_\alpha^i\delta_i^2 + \left(p^i G_\alpha^i\right)^2\frac{\delta_i^3}{3}\right) \qquad \textbf{(2.33)}$$

where we have written

$$\sum_{r=1}^{i-1} p^r s_\alpha^r = \mathbf{p}^{i-1}\mathbf{s}_\alpha^{i-1} \qquad \textbf{(2.34)}$$

for simplicity.

The second part of the integration over the time interval Δ_i is independent of the gradient shape function equal to

$$\int_{\tau_i-\Delta_i}^{\tau_i-\delta_i}\left|\gamma_I\sum_{r=1}^{i-1}p^r s_\alpha^r\right|^2 du = \left(\gamma_I\mathbf{p}^{i-1}\mathbf{s}_\alpha^{i-1}\right)^2(\Delta_i-\delta_i) \qquad \textbf{(2.35)}$$

Introducing the wavevectors $\mathbf{k}_{i-1}$ and $\mathbf{h}_i$, defined in analogy to (2.15)

$$\mathbf{k}_{i-1} = \gamma_I\sum_{r=1}^{i-1}p^r\begin{pmatrix}s_x^r\\ s_y^r\\ s_z^r\end{pmatrix} \qquad \mathbf{h}_i = \gamma_I p^i\begin{pmatrix}s_x^i\\ s_y^i\\ s_z^i\end{pmatrix} \qquad \textbf{(2.36)}$$

The attenuation of a coherence transfer pathway during the interval Δ_i is given by adding the two contributions (2.33) and (2.35)

$$\frac{S(\mathbf{k}_i)}{S_0} = \exp\left\{-D\left(\left(\mathbf{k}_{i-1}\right)^2\Delta_i + \left(\mathbf{k}_{i-1}\right)\mathbf{h}_i\delta_i + \left(\mathbf{h}_i\right)^2\frac{\delta_i}{3}\right)\right\} \qquad \textbf{(2.37)}$$

where we have assumed isotropic diffusion for simplicity.

There are three contributions to the signal attenuation during the interval Δ_i:

1. The first factor corresponds to a decay that is linear in time. The time interval Δ_i starts at the end of gradient i and ends at the end of the next gradient i+1. At the end of the integral i each coherence pathway p has accumulated a phase $\sim\Sigma p_i s_i$ corresponding to a wavevector k_i. The wavelength $\lambda_i=2\pi k_i^{-1}$ corresponds to a real spatial modulation of the magnetization in the sample. Thus a magnetization grid (Kimmich, 1997; Simon, 1996) or grating (Sodickson, 1998) is present in all three spatial dimensions. The influence of the diffusion is to reduce the amplitude of this magnetization grid by a factor $\exp(-D(k_i r_0)^2\Delta_i)$.
2. The third factor is proportional to the third power of the gradient pulse length. It depends on the coherence order during interval i and the gradient strength only, and is especially independent of any gradients applied before interval i. Due to the square, this factor is always positive leading to a signal decay. It corresponds to the unavoidable signal loss in the presence of a gradient.
3. The second factor is proportional to the product of the wavevector present before the gradient i with the gradient strength of gradient i. The sign of the product depends on the relative sign of k_{i-1} and h_i. If h_i and k_{i-1} have opposite signs this factor is negative and thus increases the signal amplitude. In words of the magnetization grid, h_i and k_{i-1} having opposite sign means that the gradient i starts to unwind the magnetization grid present over the sample.

The summation over all intervals i of the pulse-sequence results in an attenuation factor, which is just the product of the attenuation, factors for single intervals.

$$\frac{S(\mathbf{k})}{S_0} = \prod_{i=1}^{F} \exp\left\{ -D\left((\mathbf{k}_{i-1})^2 \Delta_i + (\mathbf{k}_{i-1})\mathbf{h}_i \delta_i + (\mathbf{h}_i)^2 \frac{\delta_i}{3} \right) \right\} \qquad \textbf{(2.38)}$$

The wavevector $\mathbf{k}_0 = 0$ is introduced in this formula for simplicity.
If diffusion during the gradients is neglected, e. g. taking the shape-function f to be the δ-function reproduces the result in (Jerschow, 1998). Using (2.38), the echo attenuation in pulsed field gradient stimulated echo experiments (Stejskal and Tanner, 1965) and the bipolar (Wu, 1995) or convection compensated (Jerschow, 1997) variants are easily derived.

Sine shaped gradients

Very often the shape of the pulsed field gradients is smoothed, to reduce the mechanical momentum on the gradient coil during the switching. (The strong mechanical force on the probe manifests itself in a hearable clicking, when pulsed field gradients are applied.) A very popular shape is to use the first lobe of a sine wave:

$$f_\alpha^i(t) = f(t) = \begin{cases} \sin\left(\frac{\pi}{\delta_i}(t - \tau_i + \delta_i)\right) & \tau_i - \delta_i \le t \le \tau_i \\ 0 \quad \text{otherwhise} \end{cases} \qquad \textbf{(2.39)}$$

The diffusion during the gradient is obtained in analogy to (2.33)

$$\begin{aligned} &\int_{\tau_i-\delta_i}^{\tau_i} \left| \gamma_I \left(\sum_{r=1}^{i-1} p^r s_\alpha^r + p^i G_\alpha^i \int_{\tau_i-\delta_i}^{u} \sin\left(\frac{\pi}{\delta_i}(t - \tau_i + \delta_i)\right) dt' \right) \right|^2 du \\ &= \gamma_I{}^2 \left(\left(\mathbf{p}^{i-1}\mathbf{s}_\alpha^{i-1}\right)^2 \delta_i + \mathbf{p}^{i-1}\mathbf{s}_\alpha^{i-1} p^i G_\alpha^i \frac{2\delta_i^2}{\pi} + \left(p^i G_\alpha^i\right)^2 \frac{3\delta_i^3}{2\pi^2} \right) \end{aligned} \qquad \textbf{(2.40)}$$

The strength of a single sine-gradient is

$$s = G\int_0^\delta \sin\left(\frac{\pi}{\delta}t'\right) dt' = G\frac{2\delta}{\pi} \qquad \textbf{(2.41)}$$

The overall attenuation during a pulse sequence due to diffusion is

$$\frac{S(\mathbf{k})}{S_0} = \prod_{i=1}^{F} \exp\left\{ -D\left(\left(\mathbf{k}_{i-1}\right)^2 \Delta_i + \mathbf{k}_{i-1}\mathbf{h}_i\delta_i + \left(\mathbf{h}_i\right)^2 \frac{3}{8}\delta_i \right) \right\} \qquad \textbf{(2.42)}$$

which looks basically the same as in the case of rectangular gradients except for the factor 3/8 in the diffusion during the pulsed field gradients instead of 1/3 in (2.38).

Solutions for sine-shaped gradients given for a pulsed field gradient spin echo experiment with two gradient pulses (Merrill, 1993; Price and Kuchel, 1991) are reproduced by Eq. (2-42).

2.4.2 Example: Attenuation during HQQC experiment

To give an example how to use Eqs. (2.38) or (2.42) the attenuation due to diffusion for the HQQC sequence in Fig. 2.7 will be calculated and experimentally determined (for a discussion of the coherence selection see (Thomas, 1999)).

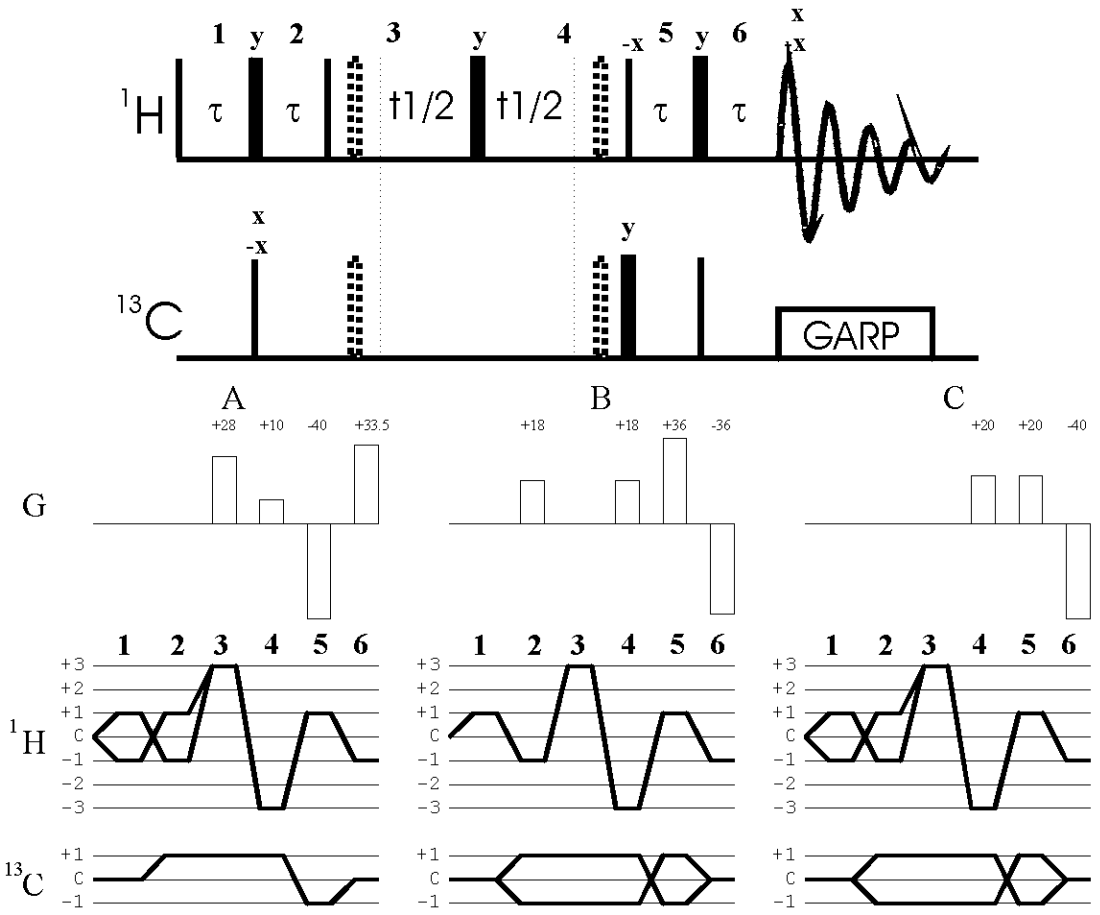

Fig. 2.7 Upper part: HQQC pulse sequence. The dotted pairs of π pulse can be added to compensate for chemical shift evolution during the gradients. Lower part: gradient sequences and selected coherence order transfer pathways. The pathways in the middle and right columns yield pure-phase data.

The gradient sequence to the left (sequence A) selects two coherence transfer pathways that have the same coherence orders during the intervals, in which gradients are applied. The attenuation of these pathways due to diffusion can be calculated by Eq. (2.42) for sine shaped gradients. The HQQC pulse sequence has six periods of free precession, thus F=6. In the intervals 1 and 2 no gradients are applied so $\mathbf{h}_1$, $\mathbf{h}_2$, $\mathbf{k}_1$ and $\mathbf{k}_2$ are equal to zero. The first gradient is applied in interval 3 with duration δ_3 and amplitude G_z^3, thus

$$s_z^3 = G_z^3 \int_0^{\delta_3} \sin\left(\frac{\pi}{\delta_3} t'\right) dt' = G_z^3 \frac{2\delta_3}{\pi} \quad s_x^3 = s_y^3 = 0$$

$$\mathbf{h}_3 = \gamma_I p^3 \begin{pmatrix} 0 \\ 0 \\ s_z^3 \end{pmatrix} = \gamma_I p^3 \begin{pmatrix} 0 \\ 0 \\ G_z^3 \frac{2\delta_3}{\pi} \end{pmatrix}$$

For the following intervals 4, 5 and 6, the corresponding wavevectors are given by

$$s_z^4 = G_z^4 \frac{2\delta_4}{\pi} \quad h_z^4 = \gamma_I p^4 G_z^4 \frac{2\delta_4}{\pi} \quad k_z^3 = h_z^3 = \gamma_I p^3 G_z^3 \frac{2\delta_3}{\pi}$$

$$s_z^5 = G_z^5 \frac{2\delta_5}{\pi} \quad h_z^5 = \gamma_I p^5 G_z^5 \frac{2\delta_5}{\pi} \quad k_z^4 = h_z^3 + h_z^4 = \gamma_I \left(p^3 G_z^3 \frac{2\delta_3}{\pi} \delta_3 + p^4 G_z^4 \frac{2\delta_3}{\pi} \delta_4 \right)$$

$$s_z^6 = G_z^6 \frac{2\delta_6}{\pi} \quad h_z^6 = \gamma_I p^6 G_z^6 \frac{2\delta_6}{\pi} \quad k_z^5 = h_z^3 + h_z^4 + h_z^5 = \gamma_I \left(p^3 G_z^3 \frac{2\delta_3}{\pi} + p^4 G_z^4 \frac{2\delta_4}{\pi} + p^5 G_z^5 \frac{2\delta_5}{\pi} \right)$$

Assuming that all pulsed field gradients have the same length δ, the overall attenuation factor is given by

$$\frac{S(\mathbf{k})}{S_0} = \prod_{i=1}^{F} \exp\left\{ -D\left((\mathbf{k}_{i-1})^2 \Delta_i + \mathbf{k}_{i-1} \mathbf{h}_i \delta + (\mathbf{h}_i)^2 \frac{3\delta}{8} \right) \right\}$$

$$= \exp\left\{ -D\left(\gamma_I \frac{2\delta}{\pi} \right)^2 \left[\left(p^3 G_z^3\right)^2 \Delta_4 + \left(p^3 G_z^3 + p^4 G_z^4\right)^2 \Delta_5 + \left(p^3 G_z^3 + p^4 G_z^4 + p^5 G_z^5\right)^2 \Delta_6 \right] \right\} \cdot$$

$$\exp\left\{ -D\left(\gamma_I \frac{2\delta}{\pi} \right)^2 \delta \left[\left(p^3 G_z^3\right)\left(p^4 G_z^4\right) + \left(p^3 G_z^3 + p^4 G_z^4\right)\left(p^5 G_z^5\right) + \left(p^3 G_z^3 + p^4 G_z^4 + p^5 G_z^5\right)\left(p^6 G_z^6\right) \right] \right\} \cdot$$

$$\exp\left\{ -D\left(\gamma_I \frac{2\delta}{\pi} \right)^2 \frac{\delta}{3} \left[\left(p^3 G_z^3\right)^2 + \left(p^4 G_z^4\right)^2 + \left(p^5 G_z^5\right)^2 + \left(p^6 G_z^6\right)^2 \right] \right\}$$

Plugging in the numbers for the gradient amplitudes G (in % of the maximum gradients strength g) and the coherence orders p, this is equal to

$$\frac{S(\mathbf{k})}{S_0} = \exp\{ -D\left(g\gamma_I \frac{2\delta}{\pi} \right)^2 [0.83\Delta_4 + 0{,}40\Delta_5 + 0.11\Delta_6 - \delta(0.25 + 0.19 + 0.11)$$

$$+ \frac{3\delta}{8}(0.82 + 0.08 + 0.09 + 0.11)]$$

$$= \exp\left\{ -D\left(g\gamma_I \frac{2\delta}{\pi} \right)^2 [0.83\Delta_4 + 0.40\Delta_5 + 0.11\Delta_6 - 0.14\delta] \right\}$$

The corresponding calculations for the three gradient sequences are summarized in Tab. 2.8.

	Free precession interval 1	2	3	4	5	6
Gradient sequence A						
G_z^i [%]	0	0	28	10	-40	33,5
Selected coherence order pathways						
${}^1p^I$	1	-0.75	3.25	-2.75	0.75	-1
${}^2p^I$	-1	1.25	3.25	-2.75	0.75	-1
Contributions to diffusion attenuation						
$(\Sigma p^{i-1}G_z^{i-1})^2$	0	0	0	0.8281	0.4032	0.1122
$(\Sigma p^{i-1}G_z^{i-1})p^iG_z^I$	0	0	0	-0.2503	0.0825	0.1005
$(p^iG_z^i)^2$	0	0	0.8281	0.0756	0.0900	0.1122
Total signal attenuation						
$S(k)/S(0)=2*\exp\{-D(g\gamma_l 2\delta/\pi)^2[0.83\Delta_4+0.40\Delta_5+0.11\Delta_6-0.14\delta]\}$						
Gradient sequence B						
G_z^i [%]	0	18	0	18	36	-36
Selected coherence order pathways						
${}^1p^I$	1	-0.75	3.25	-2.75	0.75	-1
${}^5p^I$	1	-1.25	2.75	-3.25	1.25	-1
Contributions to diffusion attenuation						
$(\Sigma^1p^{i-1}G_z^{I-1})^2$	0	0	0.0182	0.0182	0.3969	0.1296
$(\Sigma^5p^{i-1}G_z^{I-1})^2$	0	0	0.0506	0.0506	0.6561	0.1296
$(\Sigma^1p^{i-1}G_z^{I-1})p^iG_z^i$	0	0	0	0.0668	-0.1701	-0.1296
$(\Sigma^5p^{i-1}G_z^{I-1})p^iG_z^i$	0	0	0	0.1316	-0.3645	-0.1296
$({}^1p^iG_z^i)^2$	0	0.0182	0	0.2450	0.0729	0.1296
$({}^5p^iG_z^i)^2$	0	0.0506	0	0.3422	0.2025	0.1296
Total signal attenuation						
$S(k)/S(0)=\exp\{-D(g\gamma_l 2\delta/\pi)^2[(0.02)(\Delta_3+\Delta_4)+(0.40)\Delta_5+0.13\Delta_6-0.07\delta]\}$						
$+\exp\{-D(g\gamma_l 2\delta/\pi)^2[(0.05)(\Delta_3+\Delta_4)+(0.66)\Delta_5+0.13\Delta_6-0.09\delta]\}$						
Gradient sequence C						
G_z^i [%]	0	0	0	20	20	-40
Selected coherence order pathways						
${}^1p^I$	1	-0.75	3.25	-2.75	0.75	-1
${}^2p^I$	-1	1.25	3.25	-2.75	0.75	-1
${}^5p^I$	1	-1.25	2.75	-3.25	1.25	-1
${}^6p^I$	-1	0.75	2.75	-3.25	1.25	-1
Contributions to diffusion attenuation						
$(\Sigma^1p^{i-1}G_z^{I-1})^2$	0	0	0	0	0.3025	0.1600
$(\Sigma^5p^{i-1}G_z^{I-1})^2$	0	0	0	0	0.4225	0.1600
$(\Sigma^1p^{i-1}G_z^{I-1})p^iG_z^i$	0	0	0	0	-0.0825	-0.1600
$(\Sigma^5p^{i-1}G_z^{I-1})p^iG_z^i$	0	0	0	0	-0.1625	-0.1600
$({}^1p^iG_z^i)^2$	0	0	0	0.3025	0.0225	0.1600
$({}^5p^iG_z^i)^2$	0	0	0	0.4225	0.0625	0.1600
Total signal attenuation						
$S(k)/S(0)=2*\exp\{-D(g\gamma_l 2\delta/\pi)^2[(0.30)\Delta_5+0.16\Delta_6-0.06\delta]T^2m^{-2}\}$						
$+2*\exp\{-D(g\gamma_l 2\delta/\pi)^2[(0.42)\Delta_5+0.16\Delta_6-0.08\delta]T^2m^{-2}\}$						

Tab. 2.8 Equations for the signal attenuation due to diffusion for the pulse and gradient sequences of Fig. 2.7.

The time interval τ in the HQQC sequence is determined by the size of the heteronuclear proton carbon coupling constant ($\tau=(2^1J_{CH})^{-1}$). The duration of the time

intervals Δ_3-Δ_6 depends on the position of the gradients during the free precession periods. This will determine which of the intervals Δ_3-Δ_5 change by incrementing the indirect evolution interval (remember that the interval Δ_i *ends* at the end of the gradient placed in the free precession period i).

For gradient sequence B and C the coherence orders of the selected pathways are not equal during the intervals of free precession with applied gradient. The corresponding pathways are attenuated differently. Gradient sequences B and C select +0.25 and -0.25 carbon coherence order during the indirect evolution interval t1. The two pathways (p- and n-type) are necessary to get pure phase spectra in ω1.

As experimental example, HQQC spectra of ethanol in D_2O were recorded using gradient sequences A, B and C. All sequences select the signal of the ^{13}C bound methyl protons efficiently (see Fig. 2.8). The t1-ridge at the position of the ^{12}C bound methyl-proton resonance in gradient sequence B is caused mainly by instabilities of the gradient unit during some of the FIDs between t1=40ms and t1=80ms. The inspection of the signal decay with respect to t1 shows immediately the strong influence of diffusion in gradient sequence A. The additional modulation of the signals is caused by small proton-proton couplings of the methyl and methylene protons. After two-dimensional Fourier transform, pure absorption peaks in both dimensions are observed in gradient sequence B and C, because they select p- and n-type coherence orders in t1 simultaneously. The intensity of the signals reflects approximately the different number of coherence transfer pathways selected. To make a quantitative comparison, the magnitude of the two-dimensional spectrum was calculated, and all points within a box around the signals were summed up. The resulting volume ratios are 1.0 : 1.2 : 2.2 for sequence A : B : C.

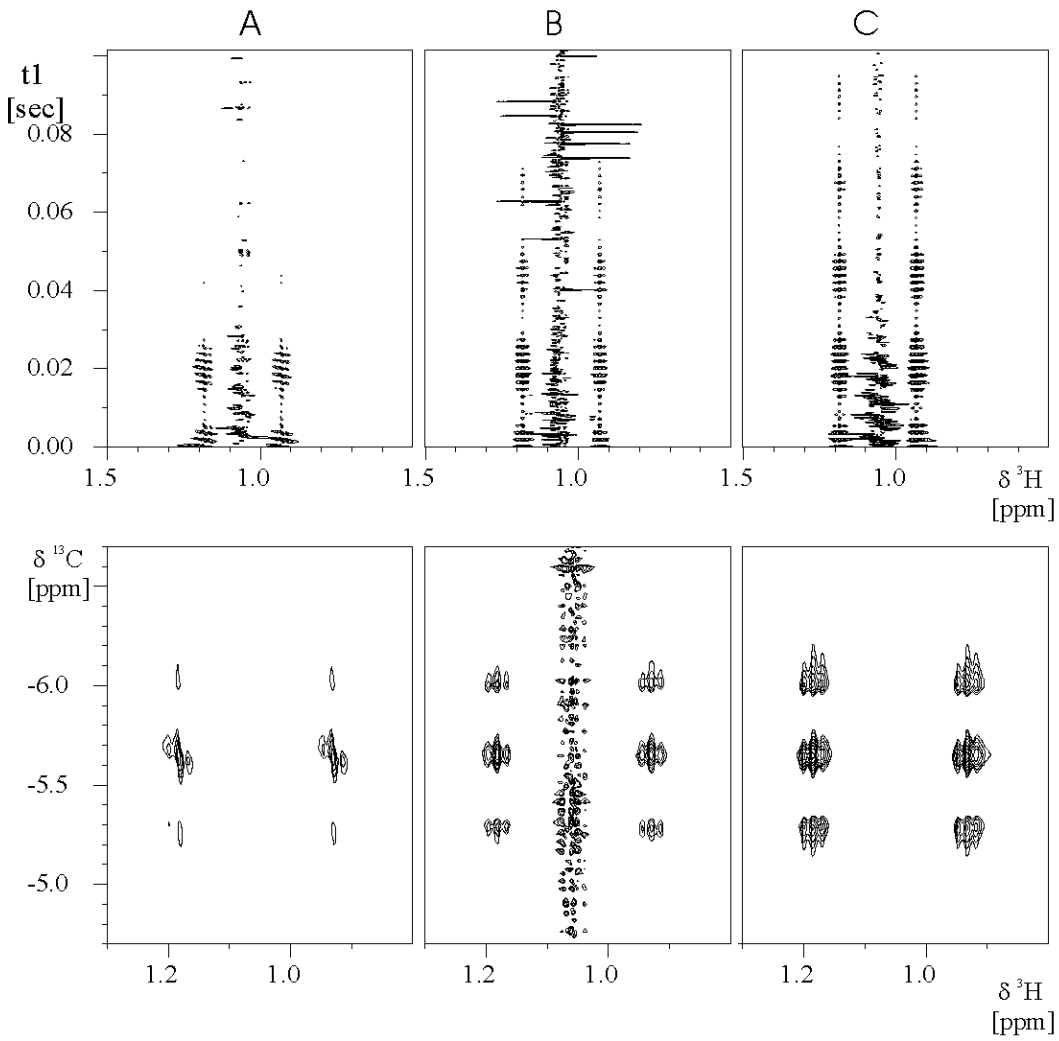

Fig. 2.8 Natural abundance ^{13}C HQQC experiment of ethanol in D_2O (containing a trace of $CuSO_4$ to enhance relaxation) using the pulse sequence in Fig. 2.7 with the optional pairs of π pulses during t1. Upper row: two-dimensional interferogram obtained after Fourier transformation with respect to the acquisition dimension. Lower trace: methyl region of the 2D spectrum. The spectra have acquired with the same number of transients, are processed identically and plotted with using the same (positive) contour levels.

The strongest influence of diffusion is observed in gradient sequence A. The first gradient is applied during a period were quadruple quantum coherence is excited, leading to a multiplication factor of 3.25 in the calculation of the effective gradient strength. The magnetization grid produced by this gradient is refocused only after the indirect evolution time t1. In gradient sequence B the attenuation during t1 is much less because the first gradient is applied in an interval during which heteronuclear double quantum coherence is excited. The attenuation in gradient sequence C is independent of t1 since the first gradient is applied after the indirect evolution period.

The difference in linewidth between the signals in the indirect dimension of spectra A and C can be used directly to determine the diffusion coefficient of ethanol. The signal decay in sequence C is governed by transverse relaxation only, while the additional linewidth in sequence A and B is caused by diffusion. The linewidth of the signals in ω2 was determined by fitting a Lorentzian to one-dimensional traces of the spectrum. The obtained values are 5.9 Hz (A), 3.7 Hz (B) and 3.6 Hz (C).

To point out the similarity between the signal loss by relaxation and diffusion, a "diffusional relaxation rate $R_d=1/T_d$" might be introduced. The interval Δ4 in the above notation is proportional to t1, and the signal decay in dependence of t1 is (see Tab. 2.8)

$$R_d = 0.83\ D\ (g\gamma_I 2\delta/\pi)^2$$

for gradient sequence A. From the experimentally determined difference of 2.3 Hz between spectrum A and C a diffusional relaxation rate $R_d=\pi\Delta\nu$ of 7.2 s^{-1} results. With the maximum gradient strength of the probehead g= 0.56 T/m, the gradient duration δ=1ms and the gyromagnetic ratio of the protons $\gamma_I=2.675\ 10^8 radT^{-1}s^{-1}$, the diffusion coefficient for ethanol is determined to be 0.96 10^{-9} m^2s^{-1}. This compares to 1.02 10^{-9} m^2s^{-1} obtained on the same sample with a stimulated echo sequence.

2.5 Discussion

Gradient selection of coherence transfer pathways must meet several practical requirements to be useful for routine NMR spectroscopy. Most importantly, the gradient sequences should guarantee that the actual NMR experiment is the one required, in the sense that only wanted signals are captured and simultaneously the unwanted ones are suppressed. The optimum solution to this problem depends on additional requirements, like maximizing the signal-to-noise ratio, obtaining pure-phase spectra in the indirect dimension, reducing the experimental time or suppressing artifacts efficiently. Not all of these criteria can be fulfilled optimally at the same time, for example maximizing signal-to-noise and reducing the experimental time are mutually exclusive, and so the selection of a particular sequence of pulsed field gradients depends on the specific application.

The computer programs TRIPLE GRADIENT and Z GRADIENT are powerful tools for the design of optimal sequences of pulsed field gradients. The number and kind of pathways to be selected or suppressed are chosen by the spectroscopist, and the programs then determine whether or not any appropriate gradient sequence exists. The programs can also be used iteratively, as described in a previous publication (Thomas, 1999), where we focus on the optimization of signal-to-noise ratio for an experiment, which excites high order coherence. The process of selecting an optimal subset of the coherence transfer pathways is outlined, which allows to record pure phase absorption peaks in the indirect dimension without any special processing.

In chapter 2.3 of this thesis, a different aspect of the design of gradient pulse sequences is addressed, namely the suppression of artifacts. With the aid of the programs TRIPLE GRADIENT and Z GRADIENT, this can be achieved after identifying the coherence transfer pathway causing the artifact. The computer programs are able to find a gradient sequence, which suppresses the unwanted pathways optimally, while the wanted signal is fully retained in cases where this is possible.

The main source of systematic artifacts in NMR spectra are imperfections of π pulses. To find the resulting unwanted pathways, we expand the pulse flip angle in a Taylor series around its nominal value and consider only the linear term. This reduces the number of unwanted pathways considerably, but retains the most important ones. For the solvent signal, the same approach is extended to all pulses and different weight factors reflecting the intensity difference of solvent and protein signal are tested. The calculated gradient sequences produce artifact free spectra with very good water suppression. The residual small water signal is caused mainly by radiation damping (which is the direct coupling of the strong water magnetization to the resonance circuit of the probehead). For further improvements of the gradient sequences it is necessary to add unwanted pathways created by radiation damping rather than including pathways caused by second order deviations of the pulse flip angles.

The application of pulsed field gradients leads to a spatial phase dependence, which is determined by the gradient sequence and the coherence orders during the experiment. The selection of a particular coherence transfer pathway is equivalent to the condition that this spatial dependence is refocused before signal acquisition and thus a gradient

echo is formed. The intensity and phase of the selected signals are changing, if the molecules undergo motion during the experiment. The theoretical part outlined in chapter 2.2 includes a very general formulation to include motional effects and following the treatment of Stepisnik (Stepisnik, 1981; Stepisnik, 1985) the equations are further analyzed using the cumulant expansion theorem.

The influence of unrestricted diffusion on the signal amplitudes in an arbitrary pulse sequence with sine pulsed field gradients (including constant gradients as a special case of a sequence of rectangular gradients with constant amplitude and no spacing) is evaluated for the first time in a general and exact way in chapter 2.4. Previously used approximations, as for example neglecting diffusion during the gradients (Jerschow, 1998), are unnecessary since the exact calculation does not require significantly more computation time.

In the experimental examples different aspects of signal selection and signal attenuation by diffusion are shown in a pulse sequence selecting heteronuclear quadruple quantum coherence. The relative signal volumes in spectra recorded with different sequences of pulsed field gradients in an otherwise identical pulse sequence is determined by the different numbers of coherence transfer pathways selected. Pure absorption peaks shapes in the spectra are only obtained of p- and n-type coherences are selected simultaneously. The signal decay in the indirect dimension is determined by transverse relaxation and diffusion. The diffusion constant of ethanol is reproduced with an accuracy of 10% from the difference in linewidth observed in the spectra.

It is expected that the formalism is going to be helpful for the design of pulse sequences to measure diffusion. The formal introduction of a “diffusional relaxation” time T_d makes clear that such experiments might use the same principles as used for the measurement of transverse or longitudinal relaxation times. Intervals used to encode for chemical shift can be used simultanesously to determine diffusion constants. In the experimental example (chapter 2.4.2) the separation of diffusion and relaxation effects is achieved by evaluating the difference of two experiments. Alternatively, a constant time chemical shift interval can be used in between gradients encoding for diffusion. If now the gradient strength and the chemical shift evolution are varied in a concerted manner, the diffusion coefficient is determined directly from the observed linewidth of the signals as in the so-called accordion approach for

measuring relaxation (Ernst, 1987). This would allow the separation of signals of different molecules in a mixture based on the diffusion coefficient from one two-dimensional experiment and thus making use of the higher resolution of the two-dimensional spectrum without extra experimental time needed for the variation of the strength of a diffusion encoding gradient used in proposed experiments (Barjat *et al*., 1998).

To improve the calculation of optimized sequences of pulsed field gradients, the influence of diffusion could be added to the penalty function of TRIPLE GRADIENT and Z GRADIENT. This should lead to better results in two different ways: (1) The diffusion losses for the wanted signals are minimized. (2) The suppression of solvent is optimized by making use of the faster diffusion of the solvent molecules compared to the molecules of interest.

The theory is formulated to allow arbitrary random or coherent motion for the spins. This makes it possible to include other motional effects than unrestricted diffusion. An analytical solution of the influence of the gradients on signal amplitude and phase is impossible in most cases and approximations have to be introduced, the most common one being the narrow (gradient) pulse approximation (Callaghan, 1991). Examples for expressions for pulsed gradient and double pulsed gradient stimulated echo experiments are found in (Callaghan, 1999).

2.6 References

Aliteri, A.S., Miller, K. E. and Byrd, R. A. (1996) A comparison of water suppression techniques using pulsed field gradients for high-resolution NMR of biomolecules. *Magn. Reson. Rev.*, **17**, 27-82.

Aue, W.P., Bartholdi, E. and Ernst, R.R. (1976) Two-dimensional spectroscopy. Application to nuclear magnetic resonance. *J. Chem. Phys.*, **64**, 2229-2246.

Bain, A.D. (1984) Coherence Levels and Coherence Pathways in NMR. A simple Way to design Phase Cycling Procedures. *J. Magn. Reson.*, **56**, 418.

Barjat, H., Morris, G.A. and Swanson, A.G. (1998) A three-dimensional DOSY-HMQC experiment for the hig-resolution analysis of comples mixtures. *J. Magn. Reson.*, **131**, 131-138.

Bax, A.and Pochapsky, S. S. (1992) Optimized recording of heteronuclear multidimensional NMR spectra using pulsed field gradients. *J. Magn. Reson.*, **99**, 638-643.

Blümich, B., Blümler, P., Botto, R. and Fukushima, E. (1998) *Spatially resolved magnetic resonance*. Wiley-VCH, Weinheim.

Bodenhausen, G., Koegler, H. and Ernst, R. R. (1984) Selection of Coherence-Transfer Pathways in NMR Pulse Experiments. *J. Magn. Reson.*, **58**, 370.

Brondeau, J., Boudot, D., Mutzenhardt, P and Canet, D. (1992) The equivalent of the DQF-COSY experiment, with one transient per t_1 value, by use of B_1 gradients. *J. Magn. Reson.*, **100**, 611-618.

Callaghan, P.T. (1991) *Principles of Nuclear Magnetic Resonance Microscopy*. Oxford University Press, Oxford.

Callaghan, P.T. and Stepisnik, J. (1995) Frequency-domain analysis of spin motion using modulated-gradient NMR. *J. Magn. Reson. Ser. A*, **117**, 118-122.

Callaghan, P.T., Codd, S.L. and Seymour, J.D. (1999) Spatial coherence phenomena arising from translational spin motion in gradient spin echo experiments. *Conc. Magn. Reson.*, 11, 181-202.

Canet, D. (1997) Radiofrequency field gradient experiments. *Prog. NMR spectr.*, **30**, 101-135.

Carr, H.Y. and Purcell, E.M. (1954) Effects of diffusion on free precession in nuclear magnetic resonance experiments. *Phys. Rev.*, **94**, 630-638.

Cavanagh, J., Fairbrother, W. J., Palmer III, A. G. and Skelton, N. J. (1996) *Protein NMR spectroscopy - principles and practice*. Academic Press, San Diego.

Cavanagh, J., Palmer III, A.G., Wright, P.E. and Rance, M. (1991) Sensitivity improvement in proton-detected two-dimensional heteronuclear relay spectroscopy. *J. Magn. Reson.*, **91**, 429-36.

Counsell, C.J.R., Levitt, M. H. and Ernst, R. R. (1985) The selection of coherence-transfer pathways by inhomogeneous z pulses. *J. Magn. Reson.*, **64**, 470-478.

Czisch, M., Ross, A., Cieslar, C. and Holak, T.A. (1996) Some practical aspects of B_0 gradient pulses. *J. Biomol. NMR*, **7**, 121-130.

Ernst, R.R. and Anderson, W.A. (1966) *Rev. Sci. Instr.*, **37**, 93-102.

Ernst, R.R., Bodenhausen, G. and Wokaun, A. (1987) *Principles of Nuclear Magnetic Resonance in One and Two Dimensions*. Clarendon Press, Oxford.

Gardiner, C.W. (1983) *Handbook of stochastic methods*. Springer, Berlin.

Gryk, M.R., Abseher, R., Simon, B., Nilges, M. and Oschkinat, H. (1998) Heteronuclear relaxation study of the PH domain of β-spectrin: Restriction of loop motions upon binding inositol trisphosphate. *J. Mol. Biol.*, **280**, 879-896.

Hahn, E.L. (1950) Spin Echos. *Phys. Rev.*, **80**, 580-594.

Hammarström, A.and Otting, G. (1994) Axial-peak artifacts in multipulse NMR experiments. *J. Magn. Reson. A*, **109**, 246-249.

Hore, P.J. (1989) In N. J. O. a. T. L. James (ed.) *Nuclear magnetic resonance. Solvent suppression.* Academic Press, San Diego, Vol. 176, pp. 64.

Hoult, D.I. (1979) Rotating Frame Zeugmatography. *J. Magn. Reson.*, **33**, 183-197.

Humbert, F., Valtier, M., Retournard, A. and Canet, D. (1998) Diffusion measurements using radiofrequency field gradient: artifacts, remedies, practical hints. *J. Magn. Reson.*, **134**, 245-254.

Hurd, R.E. (1990) Gradient-enhanced spectroscopy. *J. Magn. Reson.*, **87**, 422.

Hurd, R.E., Boban, K. J., Webb, P. and Plant, D (1992) Spatially selective suppression of B_1 inhomogeneity. *J. Magn. Reson.*, **99**, 632-637.

James, T.L. and McDonald, G.G. (1973) Measurement of the self-diffusion coefficient of each component in a complex system using pulsed-gradient Fourier transform NMR. *J. Magn. Reson.*, **11**, 58-61.

Jerschow, A.and Müller, N. (1997) Suppression of convection artifacts in stimulated-echo diffusion experiments. Double-stimulated-echo experiments. *J. Magn. Reson.*, **125**, 372-375.

Jerschow, A.and Müller, N. (1998) Efficient simulation of coherence transfer pathway selection by phase cycling and pulsed field gradients in NMR. *J. Magn. Reson.*, **134**, 17-29.

John, B.K., Plant, D., Heald, S.L. and Hurd, R.E. (1991) Efficient detection of C_αH-HN correlations in proteins using gradient-enhanced ^{15}N HMQC-TOCSY. *J. Magn. Reson.*, 664.

John, B.K., Plant, D. and Hurd, R.E. (1992) Improved proton-detected heteronuclear correlation using gradient-enhanced z and zz filters. *J. Magn. Reson. Ser. A*, **101**, 113-117.

Kay, L.E., Keifer, P. and Saarinen, T. (1992) Pure absorption gradient enhanced heteronuclear single quantum correlation spectroscopy with improved sensitivity. *J. Am. Chem. Soc.*, **114**, 10663-5.

Kay, L.E. (1995a) Field gradient techniques in NMR spectroscopy. *Curr. Op. Struct. Biol.*, **5**, 674-681.

Kay, L.E. (1995b) Pulsed field gradient multi-dimensional NMR methods for the study of protein structure and dynamics in solution. *Prog. Biophys. Mol. Biol.*, **63**, 277-99.

Kay, L.E., Xu, G.Y. and Yamazaki, T. (1994) Enhanced-Sensitivity triple-resonance spectroscopy with minimal H2O Saturation. *J. Magn. Reson. A*, **109**, 129-133.

Keeler, J.and Neuhaus, D (1985) Comparison and evaluation of methods for two-dimensional NMR spectra with absorption-mode lineshapes. *J. Magn. Reson.*, **63**, 454-472.

Kenkre, V.M., Fukushima, E. and Sheltraw, D. (1997) Simple solutions of the Torrey-Bloch equations in the NMR study of molecular diffusion. *J. Magn. Reson.*, **128**, 62-69.

Kessler, H., Gehrke, M. and Griesinger, C (1988) Zweidimensionale NMR-Spektroskopie, Gundlagen und Übersicht über die Experimente. *Angew. Chem.*, **100**, 507-554.

Kimmich, R. (1997) *NMR - Tomography, Diffusometry, Relaxometry*. Springer, Berlin Heidelberg New York.

Kimmich, R., Simon, B. and Köstler, H. (1995) Magnetization-grid rotating-frame imaging technique for diffusion and flow measurements. *J. Magn. Reson. A*, **112**, 7.

Lauterbur, P.C. (1973) Image formation by induced local interactions: examples employing nuclear magnetic resonance. *Nature*, **242**, 190.

Levitt, M.H. (1988) Density-operator theory of pulses and precession, in *Pulse methods in 1D and 2D liquid phase NMR* [W. S. Brey (ed.) Academic Press, pp. 111-147.

Liu, M., Mao, X., Ye, C., Huang, H, Nicholson, J. K. and Lindon, J. C. (1998) Improved WATERGATE pulse sequences for solvent suppression in NMR spectroscopy. *J. Magn. Reson.*, **132**, 125-129.

Liu, Z., Macias, M.J., Bottomley, M.J., Stier, G., Linge, J.P., Nilges, M., Bork, P. and Sattler, M. (1999) The three-dimensional structure of the HRDC domain and implications for the Werner and Bloom syndrome proteins. *Structure*, **7**,1557-1566.

Maas, W.E., Laukien, F. and Cory, D. G. (1993) Coherence selection by radiofrequency gradients. *J. Magn. Reson. A*, **103**, 115-117.

Maffei, P., Mutzenhardt, P. Retournard, A., Diter, B., Raulet, R., Brondeau, J. and Canet, D. (1994) NMR microscopy by radiofrequency field gradients. *J. Magn. Reson. A*, **107**, 40-49.

Mansfield, P. and Chapman, B. (1986) Active magnetic screening of gradient coils in NMR imaging. *J. Magn. Reson.*, **66**, 573.

Mansfield, P. and Chapman, B. (1987) Multishield active magnetic screening of coil structures in NMR. *J. Magn. Reson.*, **72**, 211.

Marion, D.and Wüthrich, K. (1983) Application of phase sensitive two-dimensional correlated spectroscopy (COSY) for measurements of ^{1}H-^{1}H spin-spin coupling constants in proteins. *Biochem. Biophys. Res. Commun.*, **113**, 967-974.

Maudsley, A.A., Wokaun, A. and Ernst, R.R. (1978) Coherence transfer echos. *Chem. Phys. Lett.*, **55**, 9-14.

McCall, D.W., Douglass, D. C. and Anderson, E. W. (1963) Self-diffusion studies by means of nuclear magnetic resonance spin-echo techniques. *Ber. Bunsenges. Physik. Chem.*, **67**, 336.

Merrill, M.R. (1993) NMR diffusion measurements using a composite gradient PGSE sequence. *J. Magn. Reson. Ser. A*, **103**, 223-225.

Metz, K.R., Boehmer, J. P., Bowers, J. L. and Moore, J. R. (1994) Rapid rotating-frame imaging using an rf pulse train (RIPT). *J. Magn. Reson. B*, **103**, 152-161.

Miller, J.B. (1998) *Prog. Nucl. Magn. Reson. Spectrosc.*, **33**, 273.

Mitschang, L., Davis, A. L., Keeler, J. and Oschkinat, H. (1992) Removal of zero-quantum interference in NOESY spectra of proteins by utilizing the natural inhomogeneity of the radiofrequency field. *J. Biomol. NMR*, **2**, 545.

Mitschang, L., Ponstingl, H., Grindrod, D. and Oschkinat, H. (1994) Geometrical representation of coherence transfer selection by pulsed field gradients in high-resolution nuclear magnetic resonance. *J. Chem. Phys.*, **102**, 3089-3098.

Mitschang, L. (1999) Signal Selection in High-Resolution NMR by Pulsed Field Gradients: I. Geometrical Analysis. *J. Magn. Reson.*

Muhandiram, D.R.and Kay, L. E. (1994) Gradient-enhanced triple-resonance three-dimensional NMR experiments with improved sensitivity. *J. Magn. Reson. B*, **103**, 203-216.

Mutzenhardt, P., Brondeau, J. and Canet, D. (1995) Selective COSY experiments with B_1 gradients. *J. Magn. Reson. A*, **117**, 278-284.

Ohtsuki, T. and Okano, K. (1982) Diffusion coefficients of interacting Brownian particles. *J. Chem. Phys.*, **77**, 1443-1450.

Palmer III, A.G., Cavanagh, J., Wright, P.E. and Rance, M. (1991) Sensitivity improvement in proton-detected two-dimensional heteronuclear correlation NMR spectroscopy. *J. Magn. Reson.*, **93**, 151-70.

Palmer III, A.G., Cavanagh, J., Byrd, R.A. and Rance, M. (1992) Sensitivity improvement in three-dimensional heteronuclear correlation NMR spectroscopy. *J. Magn. Reson.*, **96**, 416-424.

Piotto, M., Saudek, V. and Sklenar, V. (1992) Gradient-tailored excitation for single-quantum NMR spectroscopy of aqueous solutions. *J. Biomol. NMR*, **2**, 661.

Price, W.S. and Kuchel, W.P. (1991) Effect of nonrectangular field gradient pulses in the Stejskal and Tanner (diffusion) pulse sequence. *J. Magn. Reson.*, **94**, 133-139.

Ross, A., Czisch, M., Cieslar, C. and Holak, T.A. (1993) Efficient methods for obtaining phase-sensitive gradient-enhanced HMQC spectra. *J. Biomol. NMR*, **3**, 215.

Sattler, M., Schwendinger, M. G., Schleucher, J. and Griesinger, C. (1995) Novel strategies for sensitivity enhancement in heteronuclear multi-dimensional NMR experiments employing pulsed field gradients. *J. Biomol. NMR*, **5**, 11-22.

Sattler, M., Schleucher, J. and Griesinger, C. (1999) Heteronuclear multidimensional NMR experiments for the structure determination of proteins in solution employing pulsed field gradients. .

Schmieder, P. (1991) *Entwicklung und Anwendung neuer heteronuklearer NMR-spektroskopischer Methoden mit Protonendetektion*. Promotionsschrift TU München.

Shaw, G.L.and Stonehouse, J. (1996) Removing unwanted signals from HSQC spectra. *J. Magn. Reson. B*, **110**, 91-95.

Simon, B., Kimmich, R. and Köstler, H. (1996) Rotating-frame-imaging technique for spatially resolved diffusion and flow studies in the fringe field of rf probe coils. *J. Magn. Reson. A*, **118**, 78-83.

Sklenar, V., Piotto, M, Leppik, R, and Saudek, V (1993) Gradient-tailored water suppression for ^{1}H-^{15}N HSQC experiments optimized to retain full sensitivity. *J. Magn. Reson. A*, **102**, 241-245.

Sodickson, A.and Cory, D. G. (1998) A generalized k-space formalism for treating the spatial aspects of a variety of NMR experiments. *Prog. NMR Spectroscopy*, **33**, 77-108.

Solomon, I. (1959) Rotary spin echos. *Phys. Rev. Lett.*, **2**, 301-302.

Sorensen, O.W., Eich, G.W., Levitt, M.H., Bodenhausen, G. and Ernst, R.R. (1983) Product operator formalism for the description of NMR pulse experiments. *Prog. NMR Spectrosc.*, **16**, 163-192.

States, D.J., Haberkorn, R.A. and Ruben, D.J. (1982) A 2D NOE experiment with pure absorption phase in four quadrants. *J. Magn. Reson.*, **48**, 286-292.

Stejskal, E. and Tanner, J. (1965) Spin diffusion measurements: spin echoes in the presence of a time-dependent field gradient. *J. Chem. Phys.*, **42**, 288-292.

Stepisnik, J. (1981) Analysis of NMR Self-Diffusion Measurements by a Density Matrix Calculation. *Physica*, **104B**, 350-364.

Stepisnik, J. (1985) Measuring and Imaging of Flow by NMR. *Progr. NMR Spectr.*, **17**, 187-209.

Thomas, D.J., Mitschang, L., Simon, B. and Oschkinat, H. (1999) Signal Selection in High-Resolution NMR by Pulsed Field Gradients: II. The Design of Gradient Pulse Sequences. *J. Magn. Reson.*

Torrey, H.C. (1956) Bloch equations with diffusion terms. *Phys. Rev.*, **104**, 563-565.

Turner, R. and Bowley, R.M. (1986) *J. Phys. E., Sci. Instrum.*, **19**, 876.

Vlaardingerbroek, M.T. and denBoer, J.A. (1996) *Magnetic resonance imaging*. Springer, Berlin.

Vold, R.L., Waugh, J.S., Klein, M.P. and Phelps, D.E. (1968) Measurement of spin relaxation in complex systems. *J. Chem. Phys.*, **48**, 3831-3832.

Wang, L.Z., Caprihan, A. and Fukushima, E. (1995) The narrow-pulse criterion for pulsed-gradient spin-echo diffusion measurements. *J. Magn. Reson. Ser. A*, **117**, 209-219.

Wider, G. and Wüthrich, K. (1993) A simple experimental scheme using pulsed field gradients for coherence-pathway rejection and solvent suppression in phase-sensitive heteronuclear correlation spectra. *J. Magn. Reson.*, **1993**, 239-241.

Wijmenga, S.S., Steensma, E and van Mierlo, C. P. M. (1997) Doubly sensitivity-enhanced 3D HCCH-TOCSY of ^{13}C-labeled proteins in H_2O using heteronuclear cross polarization and pulsed field gradients. *J. Magn. Reson.*, **124**, 459-467.

Wu, D., Chen, A. and Johnson Jr., C. S. (1995) An improved diffusion-ordered spectroscopy experiment incorporating bipolar-gradient pulses. *J. Magn. Reson. A*, **115**, 260-264.